
Trade-off Between Efficiency and Consistency for Removal-based Explanations

Yifan Zhang*

IIIS, Tsinghua University

zhangyif21@mails.tsinghua.edu.cn

Haowei He*

IIIS, Tsinghua University

hhw19@mails.tsinghua.edu.cn

Zhiqian Tan

Department of Math, Tsinghua University

tanzq21@mails.tsinghua.edu.cn

Yang Yuan†

IIIS, Tsinghua University

Shanghai Artificial Intelligence Laboratory

Shanghai Qi Zhi Institute

yuanyang@tsinghua.edu.cn

Abstract

In the current landscape of explanation methodologies, most predominant approaches, such as SHAP and LIME, employ removal-based techniques to evaluate the impact of individual features by simulating various scenarios with specific features omitted. Nonetheless, these methods primarily emphasize efficiency in the original context, often resulting in general inconsistencies. In this paper, we demonstrate that such inconsistency is an inherent aspect of these approaches by establishing the Impossible Trinity Theorem, which posits that interpretability, efficiency and consistency cannot hold simultaneously. Recognizing that the attainment of an ideal explanation remains elusive, we propose the utilization of interpretation error as a metric to gauge inconsistencies and inefficiencies. To this end, we present two novel algorithms founded on the standard polynomial basis, aimed at minimizing interpretation error. Our empirical findings indicate that the proposed methods achieve a substantial reduction in interpretation error, up to 31.8 times lower when compared to alternative techniques³.

1 Introduction

Most existing explanation approaches are removal-based (Covert et al., 2021), which involve the sequential process of eliminating certain input features, examining the subsequent alterations in the model’s behavior, and ascertaining each feature’s impact through observation. However, most of these methods (Sundararajan et al., 2017; Lundberg & Lee, 2017) primarily focus on the original input with all features, often yielding inconsistent outcomes in alternative scenarios. Consequently, the resulting interpretations may not explain the network’s behavior consistently even in a small neighborhood of the input, as demonstrated in Fig. 3 in Appendix E.

Inconsistency is a non-trivial concern. Imagine a doctor treating a diabetic patient with the help of an AI system. The patient has features A, B, and C, representing three positive signals from various tests. The AI recommends administering 4 units of insulin with the following explanation: A, B, and C have weights 1, 1, and 2, respectively, amounting to 4 units in total. The doctor might then ask the AI: *what if* the patient only has A and B, but not C? One might expect the answer to be

*Equal Contribution.

†Corresponding Author

³Code is available at <https://github.com/962086838/neurips-2023-consistent-efficient>.

close to 2, as $A+B$ has a weight of 2. However, the network, being highly non-linear, might output a different suggestion like 3 units, explaining that both A and B have a weight of 1.5. Such inconsistent behaviors can significantly reduce the doctor's confidence in the interpretations, limiting the practical value of the AI system.

Consistency (see Definition 3.2) is certainly not the only objective for interpretability. Being equally important, efficiency is a commonly used axiom in the attribution methods (Weber, 1988; Friedman & Moulin, 1999; Sundararajan & Najmi, 2020), also called local accuracy (Lundberg & Lee, 2017) or completeness (Sundararajan et al., 2017), stating that the model's output should be equal to the network's output for the given input (see Definition 3.3). Naturally, one may ask the following question:

Q1: Can we generate an interpreting model that is both consistent and efficient?

Unfortunately, this is generally unattainable. We have proved the following theorem in Section 3:

Theorem 1(Impossible trinity, informal version). *For post-hoc interpreting models, interpretability, efficiency and consistency cannot hold simultaneously.*

A few examples following Theorem 1:

- (a) Most attribution methods are interpretable and efficient, but not consistent.
- (b) The original (deep) network is consistent and efficient, but not interpretable.
- (c) If one model is interpretable and consistent, it cannot be efficient.

However, consistency is necessary for many scenarios, leading to the follow-up question:

Q2: For consistent interpreting models, can they be approximately efficient?

The answer depends on the definition of “approximately efficient”. We introduce a new notion called *truthfulness*, which serves as a natural relaxation of efficiency, or partial efficiency. We divide the functional space of a network f into two subspaces: the readable part and the unreadable part. We call the interpreting model g truthful if it can accurately represent the readable part of f , denoted as V (see Definition 3.4). The unreadable part is not merely a “fitting error”; it truthfully represents the higher-order non-linearities in the network that our interpretation model g , even at its best, cannot cover. In short, what g conveys is true, though it may not encompass the entire truth. Due to Theorem 1, **this is essentially the best that consistent algorithms can achieve**.

Truthfulness is a parameterized notion, depending on the choice of the readable subspace. While there are theoretically infinite possible choices, we follow previous researchers on interpretability with non-linearities (Sundararajan et al., 2020; Masoomi et al., 2022; Tsang et al., 2020), using the basis that induces interpretable terms like $x_i x_j$ or $x_i x_j x_k$. These capture higher-order correlations and are easy to understand. The resulting subspace has the standard polynomial basis (or equivalently, the Fourier basis).

When truthfulness is parameterized with the polynomial basis, designing consistent and truthful interpreting models is equivalent to learning the Fourier spectrum (see Algorithm 1 and Lemma A.4). However, exact consistency is not always necessary for most real-world applications, as approximate consistency is usually sufficient. We formally use the number of different interpreting models (in log scale) as a metric for inconsistency. Our last question is:

Q3: When a little inconsistency is allowed, can we get better interpreting models?

We affirmatively answer this question in Section 5 by introducing a new algorithm called Harmonica-local. We then apply it multiple times to develop Harmonica-anchor and Harmonica-anchor-constrained, which offer smaller interpretation errors with a small degree of inconsistency.

In this paper, we focus on removal-based explanations (Covert et al., 2021), which implies that f and g are Boolean functions. We remark that empirically most networks are not Boolean functions, i.e., the input variables are real valued. However, for every explanation algorithm (including LIME (Ribeiro et al., 2016) and SHAP (Lundberg & Lee, 2017)) in the removal-based framework, the input x is not modified to an arbitrary real value. Instead, x is fixed, and the algorithm only retain or remove each feature of x for generating the explanations. When x is fixed with n features, it becomes natural to

use Boolean functions to represent both the network f and the interpreting model g for their outputs in all 2^n feature-removal scenarios. In other words, the algorithms in the framework only consider a fixed x each time, and given this x , there are only 2^n possible outcomes, even for the models with real inputs. Therefore, treating f and g as Boolean functions is not a simplification, but an accurate characterization of the removal-based framework (see Fig. 1 in (Covert et al., 2021) for an illustration).

Our new algorithms, including Harmonica-local, Harmonica-anchor, and Harmonica-anchor-constrained, are all based on the Harmonica algorithm from Boolean functional analysis (Hazan et al., 2018), which has rigorous theoretical guarantees on recovery performance and sampling complexities. In Section 6, we demonstrate that on datasets like IMDb and ImageNet, our algorithms achieve up to 31.8x lower interpretation error compared with other methods.

In summary, our contributions are:

- We prove the impossible trinity theorem for interpretability, demonstrating that interpretable algorithms cannot be consistent and efficient simultaneously.
- When a small inconsistency is allowed, we propose new algorithms using Harmonica-local and empirically demonstrate that these algorithms achieve significantly lower interpretation errors compared with other methods.
- For interpretable algorithms that are consistent but not efficient, we introduce a new notion called truthfulness, which can be regarded as partial efficiency. Due to the impossible trinity theorem, this is the best achievable outcome when consistency is required.

2 Related Work

Interpretability is a critical topic in machine learning, and we refer the reader to (Doran et al., 2017; Lipton, 2018) for insightful general discussions. Below we discuss different types of interpretable models.

Removal-based explanations (Covert et al., 2021) presents a unified framework for removal-based model explanation methods, connecting 26 existing techniques such as LIME (Ribeiro et al., 2016), SHAP (Lundberg & Lee, 2017), Meaningful Perturbations (Fong & Vedaldi, 2017), and permutation tests (Breiman, 2001). LIME (Ribeiro et al., 2016) is a classical method that samples data points following a predefined sampling distribution and computes a function that empirically satisfies local fidelity.

The Shapley value (Shapley, 1953; Weber, 1988; Grabisch & Roubens, 1999) originates from cooperative game theory and is used to allocate the total value generated by a group of players among individual players. It is the unique kind of method that satisfies a few important properties, including efficiency, symmetry, dummy, additivity, etc. Formally, let $N = \{1, 2, \dots, n\}$ represent a set of n players, and let $v : 2^N \rightarrow \mathbb{R}$ be a characteristic function that assigns a real value to each coalition of players. The Shapley value of player i is given by:

$$\phi_i(v) = \sum_{S \subseteq N \setminus i} \frac{(n - |S| - 1)! \cdot |S|!}{n!} [v(S \cup i) - v(S)], \quad (1)$$

where $|S|$ is the number of players in coalition S , and the sum is taken over all possible coalitions S that do not include player i .

Shapley values have been extensively applied to machine learning model explanations (Lundberg & Lee, 2017; Lundberg et al., 2018; Štrumbelj & Kononenko, 2014; Sundararajan & Najmi, 2020; Wang et al., 2021a; Zhang et al., 2021; Frye et al., 2020; Yuan et al., 2021) and feature importance (Covert et al., 2020). Recent research has focused on developing efficient approximation methods for Shapley values (Lundberg & Lee, 2017; Chen et al., 2019; Ancona et al., 2019; Covert & Lee, 2021; Jethani et al., 2021; Hamilton et al., 2022; Wang et al., 2021b). Many works have generalized Shapley values to higher-order feature interactions (Owen, 1972; Grabisch & Roubens, 1999; Sundararajan et al., 2020; Masoomi et al., 2022; Tsang et al., 2020; Aas et al., 2021; Tsai et al., 2022).

Gradient-based explanations Gradient-based explanations are popular for deep learning models, such as CNNs. These methods include SmoothGrad, Integrated Gradient, GradCAM, DeepLift, LRP, etc. (Simonyan et al., 2014; Smilkov et al., 2017; Shrikumar et al., 2017; Sundararajan et al., 2017; Xu et al., 2020; Selvaraju et al., 2017; Bach et al., 2015; Shrikumar et al., 2016; Chefer et al., 2021; Montavon et al., 2017; Shrikumar et al., 2017; Schwab & Karlen, 2019). Although these methods have seen extensive use in various areas, gradient-based methods are often time-consuming and can be insensitive to random model parameterization (Adebayo et al., 2018).

Model-specific interpretable models Interpretable or white-box models are inherently ante-hoc and model-specific. One primary goal of utilizing interpretable models is to achieve inherent model interpretability. Prominent approaches include Decision Trees ((Wang et al., 2015a; Balestrieri, 2017; Yang et al., 2018)), Decision Rules ((Wang et al., 2015b; Su et al., 2015)), Decision Sets ((Lakkaraju et al., 2019; Wang et al., 2017)), and Linear Models ((Ustun & Rudin, 2014; Ustun et al., 2014)). Moreover, another research direction attempts to use an interpretable model surrogate to approximate the original black-box models. (Chen et al., 2018) employs a two-layer additive risk model for interpreting credit risk assessments. (Bastani et al., 2017) suggests an approach called model extraction that greedily learns a decision tree to approximate f . However, these methods primarily rely on heuristics and lack theoretical guarantees.

3 Our Framework on Interpretability

We consider a Hilbert space \mathcal{H} equipped with inner product $\langle \cdot, \cdot \rangle$, and induced norm $\|\cdot\|$. We denote the input space by \mathcal{X} , the output space by \mathcal{Y} , which means $\mathcal{H} \subseteq \mathcal{X} \rightarrow \mathcal{Y}$. We use $\mathcal{G} \subset \mathcal{H}$ to denote the set of interpretable functions, and $\mathcal{F} \subset \mathcal{H}$ to denote the set of machine learning models that need interpretation. In this paper, if not mentioned otherwise we focus on models that are not self-interpretable, i.e., $f \in \mathcal{F} \setminus \mathcal{G}$.

Definition 3.1 (Interpretable and Interpretation Algorithm). We call A model g is *interpretable*, if $g \in \mathcal{G}$. An *interpretation algorithm* \mathcal{A} takes $f \in \mathcal{H}, x \in \mathcal{X}$ as inputs, and outputs $\mathcal{A}(f, x) \in \mathcal{G}$ for interpreting f on x .

As we mentioned previously, for many interdisciplinary fields, the interpretation algorithm should be consistent.

Definition 3.2 (Consistent). Given $f \in \mathcal{H}$, an interpretation algorithm \mathcal{A} is *consistent* with respect to f , if $\mathcal{A}(f, x)$ remains the same (function) for every $x \in \mathcal{X}$.

Efficiency is an important property of the attribution methods.

Definition 3.3 (Efficient). A model $g \in \mathcal{H}$ is *efficient* with respect to $f \in \mathcal{F}$ on $x \in \mathcal{X}$, if $g(x) = f(x)$.

The following theorem states that one cannot expect to achieve the best of all three worlds.

Theorem 1 (Impossible Trinity for Interpretability). For any interpretation algorithm \mathcal{A} and function sets $\mathcal{G} \subset \mathcal{F} \subseteq \mathcal{H}$, there exists $f \in \mathcal{F}$ such that with respect to f , either \mathcal{A} is not consistent, or $\mathcal{A}(f, x)$ is not efficient on x for some $x \in \mathcal{X}$.

Proof. Pick $f \in \mathcal{F} \setminus \mathcal{G}$. If \mathcal{A} is consistent with respect to f , let $g = \mathcal{A}(f, x) \in \mathcal{G}$ for any $x \in \mathcal{X}$. If for every $x \in \mathcal{X}$, $g(x) = f(x)$, we know $g = f \notin \mathcal{G}$, this is a contradiction. Therefore, there exists $x \in \mathcal{X}$ such that $g(x) \neq f(x)$. \square

Theorem 1 says efficiency is too restrictive for consistent interpretations. However, being inefficient does not mean the interpretation is wrong, it can still be truthful. Recall a subspace $V \subset \mathcal{H}$ is *closed* if whenever $\{f_n\} \subset V$ converges to some $f \in \mathcal{H}$, then $f \in V$. We have:

Definition 3.4 (Truthful gap and truthful). Given a closed subspace $V \subseteq \mathcal{H}$, $g \in \mathcal{G} \subseteq V$ and $f \in \mathcal{F}$, the *truthful gap* of g to f for V is:

$$\mathbb{T}_V(f, g) \triangleq \|f - g\|^2 - \inf_{v \in V} \|f - v\|^2 \quad (2)$$

When $\mathbb{T}_V(f, g) = 0$, we say g is *truthful* for subspace V with respect to f , and we know (see e.g. Lemma 4.1 in (Stein & Shakarchi, 2009)) $\forall v \in V, \langle f - g, v \rangle = 0$.

Truthfulness means g fully captures the information in the subspace V of f , therefore it can be seen as a natural relaxation of efficiency. To characterize the interpretation quality, we introduce the following notion.

Definition 3.5 (Interpretation error). Given functions $f, g \in \mathcal{X} \rightarrow \mathcal{Y}$, the interpretation error between f and g with respect to measure μ is

$$\mathbb{I}_{p,\mu}(f, g) \triangleq \left(\int_{\mathcal{X}} |f(x) - g(x)|^p d\mu(x) \right)^{1/p} \quad (3)$$

Notice that interpretation error is only a *loss function* that measures the quality of the interpretation, instead of a metric in ℓ_p space. Therefore, μ can be a non-uniform weight distribution following the data distribution. If μ is uniform distribution over \mathcal{X} , we abbreviate $\mathbb{I}_{p,\mu}(f, g)$ as $\mathbb{I}_p(f, g)$. For real-world applications, interpreting the model over the whole \mathcal{X} is unnecessary, so μ is usually defined as a uniform distribution on the neighborhood of input x (under a certain metric), in which case we denote the distribution as \mathcal{N}_x .

4 Applying Our Framework to Removal-based Explanations

Now we focus on interpreting removal-based explanations (Lundberg & Lee, 2017; Covert et al., 2021). Removal-based explanations are post-hoc, which means they are generated based on a target network for a fixed input, by removing features from that input. There are three choices affecting the removal-based explanations: how features are removed, what behavior is analyzed after feature removal, and how to summarize the feature influence. For example, SHAP (Lundberg & Lee, 2017) considers all possible subsets of the features, and analyzes how holding out different features affects functional value, and finally summarize the differences based on the Shapley value calculation.

Therefore, removal-based explanations can be represented as Boolean functions, as feature subset $S \subseteq [n]$ can be represented as Boolean input: $f \in \{-1, 1\}^n \rightarrow \mathbb{R}$, where -1 means the specific feature $i \in S$ is removed, 1 means the specific feature is retained. We use $-1/1$ instead of $0/1$ to represent the binary variables for ease of exposition using the Fourier basis.

4.1 Fourier basis

Fourier analysis is a handy tool for analyzing Boolean functions. Due to the space limit, we defer the more comprehensive introduction on Fourier analysis for Boolean functions to Appendix A, and only present the necessary notions here.

Definition 4.1 (Fourier basis). For any subset of variables $S \subseteq [n]$, we define the corresponding Fourier basis as $\chi_S(x) \triangleq \prod_{i \in S} x_i \in \{-1, 1\}^n \rightarrow \{-1, 1\}$.

Fourier basis is also called polynomial basis in the literature. It is a complete orthonormal basis for Boolean functions, under the uniform distribution on $\{-1, 1\}^n$. We remark that this uniform distribution is used for theoretical analysis and algorithm design, and is different from the measure μ for interpretation quality assessment in Definition 3.5.

Definition 4.2 (Fourier expansion). Any Boolean function $f \in \{-1, 1\}^n \rightarrow \mathbb{R}$ can be expanded as

$$f(x) = \sum_{S \subseteq [n]} \hat{f}_S \chi_S(x),$$

where $\hat{f}_S = \langle f, \chi_S \rangle$ is the Fourier coefficient on S .

4.2 Representative algorithms

Applying the impossible trinity theorem to removal-based explanations, there are two notable algorithms on the extremes.

Shapley values: efficient but not consistent. We have introduced the definition of Shapley values in Section 2, and one of the most important properties of Shapley values is *efficiency*, i.e. $\sum_{i \in N} \phi_i(v) = v(N) - v(\emptyset)$. As Shapley value based explanations do **not** focus on consistency, its explanation is efficient only for the original input, but not for other scenarios when certain features are removed.

Harmonica: consistent but not efficient. What can we do if we want to address consistency? As mentioned in Definition 3.4, we do not expect the algorithm to be efficient, but it can still be truthful with respect to a subspace V , which is naturally represented with the polynomial basis. Therefore, in order to learn truthful explanations for given subspace V , it is natural to consider LASSO regression over the coefficients on the polynomial basis. Harmonica (algorithm 1) fulfills this requirement (Hazan et al., 2018).

Algorithm 1 Harmonica (Hazan et al., 2018)

1. Given uniformly randomly sampled x_1, \dots, x_T , evaluate them on $f: \{f(x_1), \dots, f(x_T)\}$.
2. Solve the following regularized regression problem.

$$\underset{\alpha \in \mathbb{R}^{|C|}}{\operatorname{argmin}} \left\{ \sum_{i=1}^T \left(\sum_{S, \chi_S \in C} \alpha_S \chi_S(x_i) - f(x_i) \right)^2 + \lambda \|\alpha\|_1 \right\} \quad (4)$$

3. Output the polynomial $g(x) = \sum_{S, \chi_S \in C} \alpha_S \chi_S(x)$.

We defer detailed descriptions and theoretical guarantees of algorithms to Appendix B, C and D, discussion on the comparison of our algorithms with the existing algorithms to Appendix E.

5 Trade-off Between Efficiency and Consistency

Harmonica recovers functions across the entire function space. However, in our setting, if \mathcal{N}_x is small, it is sufficient to recover a small neighborhood of the function. This inspires us to apply Harmonica to a local space instead of the entire space. By doing so, we obtain more concentrated samples in the local neighborhood. Consequently, minimizing the interpretation error in this neighborhood becomes more manageable. We refer to Harmonica with samples in the local neighborhood as Harmonica-local.

If we relax the consistency requirement, meaning that users are willing to accept minor inconsistencies in interpretations when a slight modification is made to the input, we can achieve smaller interpretation error with Harmonica-anchor, as shown in Algorithm 2. Intuitively, Harmonic-anchor applies multiple Harmonica-local algorithms to different subspaces of the input. Specifically, for a given neighborhood region \mathcal{N}_x , we now randomly select k_x bases $b_{x,i}$, ($i = 1, 2, 3, \dots, k_x$) as interpretation anchors instead of only one basis as Harmonica does. We calculate k_x interpretation models $g_{x,i}$ on each anchor and denote the coefficient of $g_{x,i}$ as $\alpha_{x,i}$. For simplicity, we omit the subscript x in the following.

The number of bases k is highly related to consistency, so we could define the log value $\log k$ to evaluate the inconsistency of the interpretation models. The minimum inconsistency value is 0, as in Harmonica ($k = 1$), while for attribution methods, the inconsistency should be almost n , which is the number of input variables. The maximum inconsistency value depends on the neighborhood region \mathcal{N}_x , since the number of interpretation models should not exceed the number of points in \mathcal{N}_x . As a special case, the Harmonica algorithm achieves 0 inconsistency, making it the most consistent algorithm.

However, if one only considers the number of different interpretation algorithms, users may still encounter a high level of inconsistency empirically when the interpretations significantly differ from one another. Thus, another critical constraint to add is the spectrum distance constraint among different interpretations on different anchors. Based on this intuition, we introduce Harmonica-anchor-constrained in Algorithm 3. In the algorithm, λ_2 serves as a penalty coefficient for the difference between g_i , and we solve the problem using iterative gradient descent. Intuitively, a larger λ_2 restricts the expressive power of the interpretation models g_i , leading to a larger interpretation error.

Discussion on universal consistency. When discussing consistency, there are two distinct settings: “global consistency” and “universal consistency.” This paper mainly focuses on global consistency (Definition 3.2), where the interpretation pertains only to input features and not to others. This scenario falls under the category of “removal-based explanations,” and most existing interpretation methods belong to this category (26 of them were discussed in Covert et al. (2021)). In contrast,

Algorithm 2 Harmonica-anchor

Input: anchor number k , model f , a distance metric function $d(\cdot, \cdot) : (\chi_S, \chi_S) \rightarrow \mathbb{R}$ which calculates distance between two anchors (e.g., Hamming distance), sampling number T , regularization coefficient λ_1

Output: interpretation models g_i with coefficients $\alpha_i \in \mathbb{R}^{|C|}, i = 1, 2, 3, \dots, k$

- 1: Fix random bases $b_i, i = 1, 2, 3, \dots, k$ as anchors
- 2: Randomly sample T bases b_1, b_2, \dots, b_T and accordingly, we calculate $f(x_1), f(x_2), \dots, f(x_T)$
- 3: Assign each basis to the anchor with minimal distance and index using $d_i = \min\{\arg\min_j d(b_i, b_j^x)\}, i = 1, 2, 3, \dots, T$ and $j = 1, 2, 3, \dots, k$
- 4: **for** $i = 1, 2, 3, \dots, k$ **do**
- 5: Solve the following regularized regression problem.

$$\arg\min_{\alpha_i \in \mathbb{R}^{|C|}} \left\{ \sum_{n=1}^T \left(\mathbb{I}(i = d_n) \left(\sum_{S, \chi_S \in C} \alpha_{i,S} \chi_S(x_n) - f(x_n) \right) \right)^2 + \lambda \|\alpha_i\|_1 \right\} \quad (5)$$

- 6: **end for**

Algorithm 3 Harmonica-anchor-constrained

Input: anchor number k , model f , a distance metric function $d(\cdot, \cdot) : (\chi_S, \chi_S) \rightarrow \mathbb{R}$ which calculates distance between two anchors (e.g., Hamming distance), sampling number T , loss balance coefficient λ_1, λ_2 , update epochs E , update rate η

Output: interpretation models g_i with coefficients $\alpha_i, i = 1, 2, 3, \dots, k$

- 1: Fix random bases $b_i, i = 1, 2, 3, \dots, k$ as interpretation anchors
- 2: Randomly initialize $\alpha_i \in \mathbb{R}^{|C|}, i = 1, 2, 3, \dots, k$
- 3: Randomly sample T bases b_1, b_2, \dots, b_T and accordingly, we calculate $f(x_1), f(x_2), \dots, f(x_T)$
- 4: Assign each basis to the anchor with minimal distance and index with $d_i = \min\{\arg\min_j d(b_i, b_j^x)\}, i = 1, 2, 3, \dots, T$ and $j = 1, 2, 3, \dots, k$
- 5: **for** $e = 1, 2, 3, \dots, E$ **do**
- 6: $L_f = \frac{1}{T} \sum_{i=1}^T \left(\sum_{S, \chi_S \in C} \alpha_{d_i, S} \chi_S(x_i) - f(x_i) \right)^2$
- 7: $L_r = \frac{1}{k} \sum_{i=1}^k \|\alpha_i\|_1$
- 8: $L_c = \frac{1}{k} \sum_{i=1}^k \|\alpha_i - \frac{1}{k} \sum_{j=1}^k \alpha_j\|_2$
- 9: Update α_i with $\alpha_i \leftarrow \alpha_i - \eta \frac{\partial(L_f + \lambda_1 L_r + \lambda_2 L_c)}{\partial \alpha_i}$
- 10: **end for**

universal consistency implies that the interpretation may depend on features different from the input features. An example of interpreting the sentence “I am happy” could be, “This sentence does not include [very], so this person is not extremely happy.” Universal consistency is more challenging than global consistency, and we hypothesize that more powerful machinery, such as foundation models, is needed (for more discussion on foundation models, please refer to Appendix E).

6 Experiments

6.1 Analysis on Polynomial Functions

To investigate the performance of different interpretation methods, we *manually* examine the output of various algorithms (LIME (Ribeiro et al., 2016), SHAP (Lundberg & Lee, 2017), Shapley Interaction Index (Owen, 1972), Shapley Taylor (Sundararajan et al., 2020; Hamilton et al., 2022), Faith-SHAP (Tsai et al., 2022), Harmonica, and Low-degree) for lower-order polynomial functions.

We observe that all algorithms can accurately learn the coefficients of the first-order polynomial. For the second-order polynomial function, only Shapley Taylor, Faith-SHAP, Harmonica, and Low-degree can learn all the coefficients accurately. For the third-order polynomial function, only Faith-SHAP, Harmonica, and Low-degree succeed. Due to space constraints, we defer the details to Appendix F.

Faith-SHAP has an intricate representation theorem, assigning coefficients to different terms under the Möbius transform. Since the basis induced by the Möbius transform is not orthonormal, it is unclear to us whether Faith-SHAP can theoretically compute the accurate coefficients for higher-order functions. However, the running time of Faith-SHAP has an exponential dependency on n , so empirically weighted sampling on subsets of features is needed (Tsai et al., 2022). This might be the main reason why our algorithms outperform Faith-SHAP in experiments on real-world datasets.

6.2 Experimental Setup

In the rest of this section, we conduct experiments to evaluate the interpretation error $\mathbb{I}_{p,\mathcal{N}_x}(f, g)$ and truthful gap $\mathbb{T}_{V_C}(f, g)$ of Harmonica and other baseline algorithms on language and vision tasks quantitatively. In our experiments, we choose 2nd order and 3rd order Harmonica algorithms, which correspond to setting C to include all terms with order at most 2 and 3.

The baseline algorithms chosen for comparison include LIME (Ribeiro et al., 2016), Integrated Gradients (Sundararajan et al., 2017), SHAP (Lundberg & Lee, 2017), Integrated Hessians (Janizek et al., 2021), Shapley Taylor interaction index, and Faith-SHAP, where the first three are first-order algorithms, and the last three are second-order algorithms.

The two language tasks we select are the SST-2 (Socher et al., 2013) dataset for sentiment analysis and the IMDb (Maas et al., 2011) dataset for movie review classification. The vision task is the ImageNet (Krizhevsky et al., 2012) for image classification. To demonstrate the capability of our interpretation framework applied to vision tasks, we have generated two examples in Fig. 1, compared with LIME, Integrated Gradients (IG), and SHAP. Note that all of these methods are applied to the same image segmentation using the SLIC superpixels (Achanta et al., 2010).

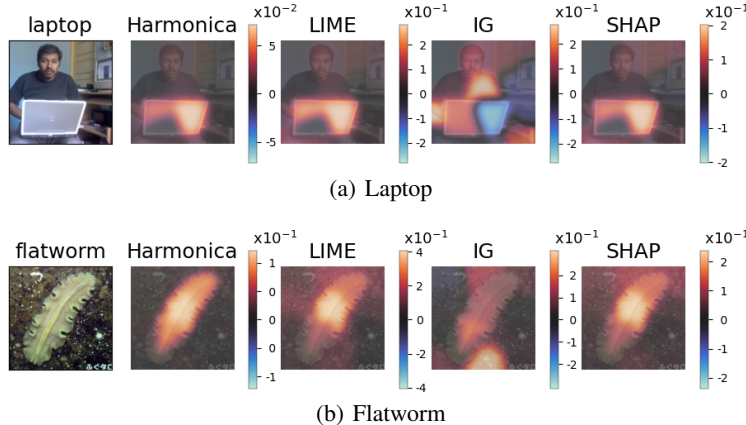


Figure 1: Illustrative examples for applying our interpretation framework to vision tasks.

For the SST-2 dataset, we attempt to interpret a convolutional neural network (see details in Appendix G) trained with the Adam (Kingma & Ba, 2015) optimizer for 10 epochs. The IMDb dataset contains long paragraphs, and each paragraph has multiple sentences. By default, we use periods, colons, and exclamation marks to separate sentences.

For ImageNet (Krizhevsky et al., 2012), we aim to provide class-specific interpretation, meaning that only the class with the maximum predicted probability is considered for each sample. Following LIME (Ribeiro et al., 2016), we split each 224×224 image into 16 superpixels to balance human readability and computational efficiency. We use the official pre-trained ResNet-101 (He et al., 2016) model from PyTorch.

6.3 Results on Interpretation Error

For a given input sentence x with length l , we define the induced neighborhood \mathcal{N}_x by introducing a masking operation on this sentence. The radius $0 \leq r \leq l$ is defined as the maximum number of masked words.

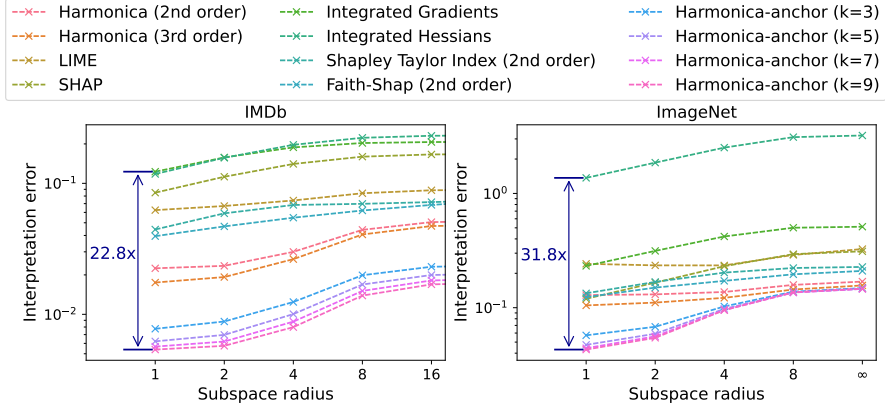


Figure 2: Visualization of L^2 interpretation error $\mathbb{I}_{p, N_x}(f, g)$ of several state-of-the-art interpretation methods evaluated on IMDb and ImageNet datasets.

Fig. 2 displays the L^2 interpretation error evaluated under different neighborhoods with a radius ranging from 1 to ∞ for all the considered datasets. Here, ∞ represents the maximum sentence length, which may vary for different data points. We also inspect L^1 and L^0 norms. Here, L^2 and L^1 are defined according to Eqn. (3) with $p = 2$ and $p = 1$, respectively. And L^0 denotes $\int_{\mathcal{X}} \mathbb{1}|f(x) - g(x)| \geq 0.1d\mu(x)$. We can see that Harmonica consistently outperforms all the other baselines on all radii.

Note that for IMDb in Fig. 2, we make a slight modification such that the masking operation is performed on sentences in one input paragraph instead (we also change the definition of radii accordingly). For ImageNet in Fig. 2, the interpretation error is evaluated on 1000 random images, and the masking operation is performed on 16 superpixels in one input image instead (we also change the definition of radii accordingly). We can see that when the neighborhood’s radius is greater than 1, Harmonica outperforms all the other baselines. Specifically, when evaluated on ImageNet dataset, Harmonica-anchor ($k = 9$) achieves 31.8 times lower interpretation error \mathbb{I}_{2, N_1} compare to Integrated Gradients (Sundararajan et al., 2017). Limited by space, the detailed numerical results and interpretation error under other norms are presented in Appendix H. In contrast, Harmonica-local achieves more accurate local consistency but high error outside the neighborhood. The relevant results are deferred in Appendix I due to limited space.

As mentioned in Section 5, Harmonica-anchor further reduces the interpretation error by learning each subspace separately. Fig. 2 shows that the L_2 interpretation error of Harmonica-anchor achieves lower error than Harmonica on various datasets, and the error further declines as we increase the number of anchors. Full results of other norms and the results of Harmonica-anchor-constrained are shown in Appendix K.

Table 1: Comparison of C^3 truthful gap $\mathbb{T}_C(f, g)$ results evaluated on IMDb and ImageNet datasets (lower truthful gap means better truthfulness of the interpretation).

Method	Harm. 2nd	Harm. 3rd	LIME	SHAP	IG	IH	Shapley Taylor	Faith- Shap
IMDb	0.540	0.174	5.343	1.390	1.438	1.948	7.005	15.528
ImageNet	0.660	0.246	0.738	2.023	1.848	175.368	0.474	0.430

6.4 Results on Truthful Gap

For convenience, we define the set of bases C^d up to degree d as $C^d = \{\chi_S | S \subseteq [n], |S| \leq d\}$. We evaluate the truthful gap on the set of bases C^3 , C^2 , and C^1 . For implementation details on calculating the truthful gap, please refer to Appendix J. Table 1 shows the C^3 truthful gap evaluated on different datasets. We can see that Harmonica outperforms all the other baseline algorithms. Due to space limitations, C^2 and C^1 results are provided in Appendix J.

6.5 Additional Experiments

We further explore Harmonica’s performance when limited to a local space instead of the whole space. The relevant discussions can be found in Appendix I.

It is worth noting that L_r is a regularization loss for Harmonica, ensuring the sparseness of each interpretation model g_i . Additionally, L_c is a regularization loss penalizing the difference between interpretation models. The value of balance coefficients depends on the application scenario and can be determined by the end user.

7 Conclusion

In this paper, we tackled the problem of generating consistent interpretations and introduced the impossible trinity theorem of interpretability, under a formal framework for understanding the interplay between interpretability, consistency, and efficiency. Since a consistent interpretation cannot be efficient, we relaxed efficiency to truthfulness, meaning the interpretation matches the target function in a specific subspace. This led to the problem of learning Boolean functions and the proposal of new algorithms based on the Fourier spectrum and a localized version of Harmonica. Our methods showed lower interpretation errors and improved consistency compared to the existing approaches.

While our work offers theoretical insights, many open questions and challenges remain in building more interpretable, consistent, and efficient models. We hope our work serves as a foundation for future research in the area of explainable AI.

Acknowledgments

Thanks to Jiaye Teng for the useful discussions. This work is supported by the Ministry of Science and Technology of the People’s Republic of China, the 2030 Innovation Megaprojects “Program on New Generation Artificial Intelligence” (Grant No. 2021AAA0150000).

References

Aas, K., Jullum, M., and Løland, A. Explaining individual predictions when features are dependent: More accurate approximations to shapley values. *Artificial Intelligence*, 298:103502, 2021. 3

Achanta, R., Shaji, A., Smith, K., Lucchi, A., Fua, P., and Süstrunk, S. Slic superpixels. Technical report, EPFL, 2010. 8

Adebayo, J., Gilmer, J., Muelly, M., Goodfellow, I., Hardt, M., and Kim, B. Sanity checks for saliency maps. *Advances in neural information processing systems*, 31, 2018. 4

Allen-Zhu, Z. and Yuan, Y. Improved svrg for non-strongly-convex or sum-of-non-convex objectives. In *International Conference on Machine Learning*, pp. 1080–1089. PMLR, 2016. 18

Ancona, M., Oztireli, C., and Gross, M. Explaining deep neural networks with a polynomial time algorithm for shapley value approximation. In *International Conference on Machine Learning*, pp. 272–281. PMLR, 2019. 3

Bach, S., Binder, A., Montavon, G., Klauschen, F., Müller, K.-R., and Samek, W. On pixel-wise explanations for non-linear classifier decisions by layer-wise relevance propagation. *PloS one*, 10(7):e0130140, 2015. 4

Balestrieri, R. Neural decision trees. *ArXiv*, abs/1702.07360, 2017. 4

Bastani, O., Kim, C., and Bastani, H. Interpretability via model extraction. *ArXiv*, abs/1706.09773, 2017. 4

Beckner, W. Inequalities in fourier analysis. *Annals of Mathematics*, 102(1):159–182, 1975. [16](#)

Breiman, L. Random forests. *Machine learning*, 45:5–32, 2001. [3](#)

Bubeck, S., Chandrasekaran, V., Eldan, R., Gehrke, J., Horvitz, E., Kamar, E., Lee, P., Lee, Y. T., Li, Y., Lundberg, S., et al. Sparks of artificial general intelligence: Early experiments with gpt-4. *arXiv preprint arXiv:2303.12712*, 2023. [20](#)

Caron, M., Touvron, H., Misra, I., Jégou, H., Mairal, J., Bojanowski, P., and Joulin, A. Emerging properties in self-supervised vision transformers. In *Proceedings of the IEEE/CVF international conference on computer vision*, pp. 9650–9660, 2021. [20](#)

Chefer, H., Gur, S., and Wolf, L. Transformer interpretability beyond attention visualization. In *Proceedings of the IEEE/CVF Conference on Computer Vision and Pattern Recognition*, pp. 782–791, 2021. [4](#)

Chen, C., Lin, K., Rudin, C., Shaposhnik, Y., Wang, S., and Wang, T. An interpretable model with globally consistent explanations for credit risk. *ArXiv*, abs/1811.12615, 2018. [4](#)

Chen, J., Song, L., Wainwright, M. J., and Jordan, M. I. L-shapley and c-shapley: Efficient model interpretation for structured data. *ArXiv*, abs/1808.02610, 2019. [3](#)

Covert, I. and Lee, S.-I. Improving kernelshap: Practical shapley value estimation using linear regression. In *International Conference on Artificial Intelligence and Statistics*, pp. 3457–3465. PMLR, 2021. [3](#)

Covert, I., Lundberg, S. M., and Lee, S.-I. Understanding global feature contributions with additive importance measures. *Advances in Neural Information Processing Systems*, 33:17212–17223, 2020. [3](#)

Covert, I., Lundberg, S. M., and Lee, S.-I. Explaining by removing: A unified framework for model explanation. *The Journal of Machine Learning Research*, 22:209–1, 2021. [1, 2, 3, 5, 6](#)

Dembo, A., Cover, T. M., and Thomas, J. A. Information theoretic inequalities. *IEEE Transactions on Information theory*, 37(6):1501–1518, 1991. [16](#)

Doran, D., Schulz, S., and Besold, T. R. What does explainable ai really mean? a new conceptualization of perspectives. *ArXiv*, abs/1710.00794, 2017. [3](#)

Fong, R. C. and Vedaldi, A. Interpretable explanations of black boxes by meaningful perturbation. In *Proceedings of the IEEE international conference on computer vision*, pp. 3429–3437, 2017. [3](#)

Friedman, E. and Moulin, H. Three methods to share joint costs or surplus. *Journal of Economic Theory*, 87(2):275–312, 1999. [2](#)

Frye, C., Rowat, C., and Feige, I. Asymmetric shapley values: incorporating causal knowledge into model-agnostic explainability. *Advances in Neural Information Processing Systems*, 33:1229–1239, 2020. [3](#)

Grabisch, M. and Roubens, M. An axiomatic approach to the concept of interaction among players in cooperative games. *International Journal of Game Theory*, 28:547–565, 1999. [3](#)

Gur, T. and Tamuz, O. Testing booleanity and the uncertainty principle. *arXiv preprint arXiv:1204.0944*, 2012. [16, 17](#)

Hamilton, M., Lundberg, S. M., Zhang, L., Fu, S., and Freeman, W. T. Axiomatic explanations for visual search, retrieval, and similarity learning. In *International Conference on Learning Representations*, 2022. [3, 7, 20](#)

Hazan, E., Klivans, A. R., and Yuan, Y. Hyperparameter optimization: A spectral approach. *ArXiv*, abs/1706.00764, 2018. [3, 6, 16, 17, 18](#)

He, K., Zhang, X., Ren, S., and Sun, J. Deep residual learning for image recognition. In *Proceedings of the IEEE conference on computer vision and pattern recognition*, pp. 770–778, 2016. [8, 22](#)

Hirschman, I. I. A note on entropy. *American journal of mathematics*, 79(1):152–156, 1957. [16](#)

Janizek, J. D., Sturmfels, P., and Lee, S.-I. Explaining explanations: Axiomatic feature interactions for deep networks. *J. Mach. Learn. Res.*, 22:104:1–104:54, 2021. [8](#)

Jethani, N., Sudarshan, M., Covert, I. C., Lee, S.-I., and Ranganath, R. Fastshap: Real-time shapley value estimation. In *International Conference on Learning Representations*, 2021. [3](#)

Kingma, D. P. and Ba, J. Adam: A method for stochastic optimization. *Arxiv*, abs/1412.6980, 2015. [8](#), [22](#)

Krizhevsky, A., Sutskever, I., and Hinton, G. E. Imagenet classification with deep convolutional neural networks. *Communications of the ACM*, 60:84 – 90, 2012. [8](#)

Kushilevitz, E. and Mansour, Y. Learning decision trees using the fourier spectrum. In *Proceedings of the twenty-third annual ACM symposium on Theory of computing*, pp. 455–464, 1991. [16](#)

Lakkaraju, H., Kamar, E., Caruana, R., and Leskovec, J. Faithful and customizable explanations of black box models. In *Proceedings of the 2019 AAAI/ACM Conference on AI, Ethics, and Society*, pp. 131–138, 2019. [4](#)

Linial, N., Mansour, Y., and Nisan, N. Constant depth circuits, fourier transform, and learnability. *Journal of the ACM (JACM)*, 40(3):607–620, 1993. [16](#), [19](#)

Lipton, Z. C. The mythos of model interpretability: In machine learning, the concept of interpretability is both important and slippery. *Queue*, 16(3):31–57, 2018. [3](#)

Lundberg, S. M. and Lee, S.-I. A unified approach to interpreting model predictions. In *Advances in Neural Information Processing Systems*, 2017. [1](#), [2](#), [3](#), [5](#), [7](#), [8](#), [20](#)

Lundberg, S. M., Erion, G. G., and Lee, S.-I. Consistent individualized feature attribution for tree ensembles. *arXiv preprint arXiv:1802.03888*, 2018. [3](#)

Maas, A., Daly, R. E., Pham, P. T., Huang, D., Ng, A. Y., and Potts, C. Learning word vectors for sentiment analysis. In *Proceedings of the 49th annual meeting of the association for computational linguistics: Human language technologies*, pp. 142–150, 2011. [8](#)

Masoomi, A., Hill, D., Xu, Z., Hersh, C. P., Silverman, E. K., Castaldi, P. J., Ioannidis, S., and Dy, J. G. Explanations of black-box models based on directional feature interactions. In *International Conference on Learning Representations*, 2022. [2](#), [3](#)

Montavon, G., Lapuschkin, S., Binder, A., Samek, W., and Müller, K.-R. Explaining nonlinear classification decisions with deep taylor decomposition. *Pattern recognition*, 65:211–222, 2017. [4](#)

O'Donnell, R. *Analysis of boolean functions*. Cambridge University Press, 2014. [15](#), [17](#)

Oquab, M., Darcet, T., Moutakanni, T., Vo, H., Szafraniec, M., Khalidov, V., Fernandez, P., Haziza, D., Massa, F., El-Nouby, A., et al. Dinov2: Learning robust visual features without supervision. *arXiv preprint arXiv:2304.07193*, 2023. [20](#)

Owen, G. Multilinear extensions of games. *Management Science*, 18(5-part-2):64–79, 1972. [3](#), [7](#)

Pennington, J., Socher, R., and Manning, C. D. Glove: Global vectors for word representation. In *Proceedings of the 2014 conference on empirical methods in natural language processing*, pp. 1532–1543, 2014. [22](#)

Ribeiro, M. T., Singh, S., and Guestrin, C. "why should i trust you?" explaining the predictions of any classifier. In *Proceedings of the 22nd ACM SIGKDD International Conference on Knowledge Discovery and Data Mining*, pp. 1135–1144, 2016. [2](#), [3](#), [7](#), [8](#), [19](#)

Schwab, P. and Karlen, W. Cxplain: Causal explanations for model interpretation under uncertainty. *Advances in Neural Information Processing Systems*, 32, 2019. [4](#)

Selvaraju, R. R., Das, A., Vedantam, R., Cogswell, M., Parikh, D., and Batra, D. Grad-cam: Visual explanations from deep networks via gradient-based localization. *International Journal of Computer Vision*, 128:336–359, 2017. [4](#)

Shapley, L. S. Quota solutions of n-person games. *Edited by Emil Artin and Marston Morse*, pp. 343, 1953. [3](#)

Shrikumar, A., Greenside, P., Shcherbina, A., and Kundaje, A. Not just a black box: Learning important features through propagating activation differences. *CoRR*, abs/1605.01713, 2016. [4](#)

Shrikumar, A., Greenside, P., and Kundaje, A. Learning important features through propagating activation differences. In *International Conference on Machine Learning*, pp. 3145–3153. PMLR, 2017. [4](#)

Simonyan, K., Vedaldi, A., and Zisserman, A. Deep inside convolutional networks: Visualising image classification models and saliency maps. *CoRR*, abs/1312.6034, 2014. [4](#)

Smilkov, D., Thorat, N., Kim, B., Viégas, F. B., and Wattenberg, M. Smoothgrad: removing noise by adding noise. *ArXiv*, abs/1706.03825, 2017. [4](#)

Socher, R., Perelygin, A., Wu, J., Chuang, J., Manning, C. D., Ng, A. Y., and Potts, C. Recursive deep models for semantic compositionality over a sentiment treebank. In *Proceedings of the 2013 conference on empirical methods in natural language processing*, pp. 1631–1642, 2013. [8](#)

Stein, E. M. and Shakarchi, R. *Real analysis: measure theory, integration, and Hilbert spaces*. Princeton University Press, 2009. [4](#)

Štrumbelj, E. and Kononenko, I. Explaining prediction models and individual predictions with feature contributions. *Knowledge and information systems*, 41(3):647–665, 2014. [3](#)

Su, G., Wei, D., Varshney, K. R., and Malioutov, D. M. Interpretable two-level boolean rule learning for classification. *ArXiv*, abs/1511.07361, 2015. [4](#)

Sundararajan, M. and Najmi, A. The many shapley values for model explanation. In *International Conference on Machine Learning*, pp. 9269–9278. PMLR, 2020. [2](#), [3](#)

Sundararajan, M., Taly, A., and Yan, Q. Axiomatic attribution for deep networks. In *International Conference on Machine Learning*, pp. 3319–3328. PMLR, 2017. [1](#), [2](#), [4](#), [8](#), [9](#), [20](#)

Sundararajan, M., Dhamdhere, K., and Agarwal, A. The shapley taylor interaction index. In *International conference on machine learning*, pp. 9259–9268. PMLR, 2020. [2](#), [3](#), [7](#), [20](#)

Tsai, C.-P., Yeh, C.-K., and Ravikumar, P. Faith-shap: The faithful shapley shapley interaction index. *arXiv preprint arXiv:2203.00870*, 2022. [3](#), [7](#), [8](#)

Tsang, M., Rambhatla, S., and Liu, Y. How does this interaction affect me? interpretable attribution for feature interactions. *Advances in Neural Information Processing Systems*, 33:6147–6159, 2020. [2](#), [3](#)

Ustun, B. and Rudin, C. Methods and models for interpretable linear classification. *ArXiv*, abs/1405.4047, 2014. [4](#)

Ustun, B., Tracà, S., and Rudin, C. Supersparse linear integer models for interpretable classification. *ArXiv*, abs/1306.6677, 2014. [4](#)

Wang, J., Fujimaki, R., and Motohashi, Y. Trading interpretability for accuracy: Oblique treed sparse additive models. In *Proceedings of the 21th ACM SIGKDD International Conference on Knowledge Discovery and Data Mining*, pp. 1245–1254, 2015a. [4](#)

Wang, J., Wiens, J., and Lundberg, S. Shapley flow: A graph-based approach to interpreting model predictions. In *International Conference on Artificial Intelligence and Statistics*, pp. 721–729. PMLR, 2021a. [3](#)

Wang, R., Wang, X., and Inouye, D. I. Shapley explanation networks. In *9th International Conference on Learning Representations, ICLR 2021, Virtual Event, Austria, May 3-7, 2021*, 2021b. [3](#)

Wang, T., Rudin, C., Doshi-Velez, F., Liu, Y., Klampfl, E., and MacNeille, P. Or's of and's for interpretable classification, with application to context-aware recommender systems. *ArXiv*, abs/1504.07614, 2015b. [4](#)

Wang, T., Rudin, C., Doshi-Velez, F., Liu, Y., Klampfl, E., and MacNeille, P. A bayesian framework for learning rule sets for interpretable classification. *The Journal of Machine Learning Research*, 18(1):2357–2393, 2017. [4](#)

Weber, R. J. Probabilistic values for games, the shapley value. essays in honor of lloyd s. shapley (ae roth, ed.), 1988. [2](#), [3](#)

Wei, J., Wang, X., Schuurmans, D., Bosma, M., Chi, E., Le, Q., and Zhou, D. Chain of thought prompting elicits reasoning in large language models. *arXiv preprint arXiv:2201.11903*, 2022. [20](#)

Xu, S., Venugopalan, S., and Sundararajan, M. Attribution in scale and space. In *2020 IEEE/CVF Conference on Computer Vision and Pattern Recognition, CVPR 2020, Seattle, WA, USA, June 13–19, 2020*, pp. 9677–9686. Computer Vision Foundation / IEEE, 2020. doi: 10.1109/CVPR42600.2020.00970. [4](#)

Yang, Y., Morillo, I. G., and Hospedales, T. M. Deep neural decision trees. *ArXiv*, abs/1806.06988, 2018. [4](#)

Yuan, H., Yu, H., Wang, J., Li, K., and Ji, S. On explainability of graph neural networks via subgraph explorations. In *International Conference on Machine Learning*, pp. 12241–12252. PMLR, 2021. [3](#)

Zhang, H., Xie, Y., Zheng, L., Zhang, D., and Zhang, Q. Interpreting multivariate shapley interactions in dnns. In *Proceedings of the AAAI Conference on Artificial Intelligence*, volume 35, pp. 10877–10886, 2021. [3](#)

A Fourier Analysis of Boolean Function

Fourier analysis of Boolean function is a fascinating field, and we refer the reader to (O'Donnell, 2014) for a more comprehensive introduction. We define the inner product as follows.

Definition A.1 (Inner product). Given two functions $f, g \in \{-1, 1\}^n \rightarrow \mathbb{R}$, their inner product is:

$$\langle f, g \rangle \triangleq \mathbb{E}_{x \sim \{-1, 1\}^n} [f(x)g(x)] = 2^{-n} \sum_{x \in \{-1, 1\}^n} f(x)g(x) \quad (6)$$

In addition, we define the induced norm $\|f\|_2 \triangleq \sqrt{\langle f, f \rangle}$, and more generally, for $p > 0$,

$$\|f\|_p \triangleq \mathbb{E}[|f(x)|^p]^{1/p}. \quad (7)$$

The inner product defines one kind of similarity between two functions and is invariant under different basis. Specifically, we have the following Theorem.

Definition A.2 (Plancherel's Theorem). Given two functions $f, g \in \{-1, 1\}^n \rightarrow \mathbb{R}$,

$$\langle f, g \rangle = \sum_{S \subseteq [n]} \hat{f}_S \hat{g}_S$$

When setting $f = g$, we get the Parseval's identity: $\mathbb{E}[f^2] = \sum_S \hat{f}_S^2$.

A distribution over a discrete domain S is often represented as a non-negative function $f : S \rightarrow \mathbb{R}^+$ which is normalized in L_1 , i.e., $\sum_{x \in S} f(x) = 1$.

Now we define the notion of C -Readable function.

Definition A.3 (C -Readable function). Given a set of Fourier bases C , a function f is C -readable if it is supported on C . That is, for any $\chi_S \notin C$, $\langle f, \chi_S \rangle = 0$. Denote the corresponding subspace as V_C .

The Readable notion is parameterized with C , because it may differ case by case. If we set C to be all the single variable bases, only linear functions are readable; if we set C to be all the bases with the degree at most 2, functions with pairwise interactions are also readable. Moreover, if we further add one higher order term to C , e.g., $\chi_{\{x_1, x_2, x_3, x_4\}}$, it means we can also reason about the factor $x_1 x_2 x_3 x_4$ in the interpretation, which might be an important empirical factor that people can easily understand. Starting from the bases set C , we have the following formula for computing the truthful gap.

Lemma A.4 (Truthful gap for Boolean functions). *Given a set of Fourier bases C , two functions $f, g \in \{-1, 1\}^n \rightarrow \mathbb{R}$, the truthful gap of g to f for C is*

$$\mathbb{T}_{V_C}(f, g) = \sum_{\chi_S \in C} \langle f - g, \chi_S \rangle^2 \quad (8)$$

Proof. Denote the complement space as $V_{\bar{C}}$. We may expand f, g, v on both bases and get:

$$\begin{aligned} \|f - g\|^2 - \inf_{v \in V} \|f - v\|_2^2 &= \sum_{S \in C} \langle f - g, \chi_S \rangle^2 + \\ &\quad \sum_{S \in \bar{C}} \langle f, \chi_S \rangle^2 - \inf_{v \in V_C} \left(\sum_{S \in C} \langle f - v, \chi_S \rangle^2 + \sum_{S \in \bar{C}} \langle f, \chi_S \rangle^2 \right) \\ &= \sum_{S \in C} \langle f - g, \chi_S \rangle^2 - \inf_{v \in V_C} \left(\sum_{S \in C} \langle f - v, \chi_S \rangle^2 \right) \\ &= \sum_{S \in C} \langle f - g, \chi_S \rangle^2 \end{aligned}$$

Where the last equality holds because we can set the Fourier coefficients $\hat{v}_S = \hat{f}_S$ for every $S \in C$, which further gives $\langle f - v, \chi_S \rangle = 0$. \square

With the previous definitions, it becomes clear that finding a truthful interpretation g is equivalent to accurately learning a Boolean function with respect to the readable bases set C . Intuitively, it means we want to find algorithms that can compute the coefficients for the bases in C . In other words, we want to find the importance of the bases like $x_1, x_2x_5, x_2x_6x_7$, etc. Learning Boolean function is a classical problem in learning theory, and there are many algorithms like KM algorithm (Kushilevitz & Mansour, 1991), Low-degree algorithm (Linial et al., 1993) and Harmonica (Hazan et al., 2018).

We pick two algorithms for our task: Harmonica (see Appendix C) and Low-degree (see Appendix D). Compared with Low-degree, Harmonica has much better sampling efficiency based on compressed sensing techniques. Specifically, for general real-valued decision trees which has s leaf nodes and are bounded by B , the sample complexity of Harmonica is $\tilde{O}(B^2 s^2 / \varepsilon \cdot \log n)$, while Low-degree is $\tilde{O}(B^4 s^2 / \varepsilon^2 \cdot \log n)$ (Hazan et al., 2018). However, the Low-degree algorithm works for more general settings, while the theoretical guarantee of Harmonica depends on the assumption that f is approximately sparse in the Fourier space. Therefore, we include both algorithms for completeness. Empirically, Harmonica has a much better performance than Low-degree (see Section 6).

B Uncertainty Principle for Boolean functions

In the field of modern physics, the state of a particle on a given domain S is represented by a complex function on that domain, and the probability of finding the particle in a specific position x on S is given by the square of the modulus of the function evaluated at x . To ensure that the function is normalized, in the case where S is continuous, the function must satisfy $\int_{x \in \mathbb{R}} |f(x)|^2 dx = 1$. The Fourier transform of the function, denoted by \hat{f} , is also normalized in L_2 under a unitary transformation, and $|\hat{f}(x)|^2$ represents the probability density function of the distribution of the particle's momentum.

The Heisenberg uncertainty principle states that the product of the variances of a particle's position and momentum is at least one, with an appropriate choice of units. This principle has physical significance and relates a function on \mathbb{R} to its Fourier transform.

In 1957, (Hirschman, 1957) proposed an entropic form of the uncertainty principle, which was later proven nearly two decades later by Beckner (Beckner, 1975). The inequality states that $H_e[f] + H_e[\hat{f}] \geq 1 - \ln 2$, where $H_e[f]$ is the differential entropy of f , defined as $-\int_{x \in \mathbb{R}} |f(x)|^2 \ln |f(x)|^2 dx$.

When the domain is \mathbb{F}_2^n (equivalently, $\{-1, 1\}^n$), a similar inequality (Gur & Tamuz, 2012) holds with a different constant. Let $f : \mathbb{F}_2^n \rightarrow \mathbb{C}$ have a Fourier transform $\hat{f} : \mathbb{F}_2^n \rightarrow \mathbb{C}$. Then,

$$H\left[\frac{f}{\|f\|}\right] + H\left[\frac{\hat{f}}{\|\hat{f}\|}\right] \geq n,$$

where $H[f] = -\sum_{x \in \mathbb{F}_2^n} |f(x)|^2 \log_2 |f(x)|^2$, and $\|f\| = \sqrt{\sum_{x \in \mathbb{F}_2^n} f(x)^2}$.

Now we present the discrete uncertainty principle for \mathbb{Z}_2^n as the following. It can be proved using Theorem 23 in Dembo, Cover, and Thomas (Dembo et al., 1991).

Theorem B.1 (The Uncertainty Principle for Boolean functions (entropy version) (Gur & Tamuz, 2012)). *For any non-zero function $f : \mathbb{F}_2^n \rightarrow \mathbb{R}$ (i.e., $\|f\| > 0$) it holds that*

$$H\left[\frac{f}{\|f\|}\right] + H\left[\frac{\hat{f}}{\|\hat{f}\|}\right] \geq n. \quad (9)$$

All the Fourier coefficients together are called the Fourier spectrum of f . We can define the following distance between two functions based on their spectrums.

Definition B.2 (Spectrum distance for Boolean functions). Given two interpretations $g(\cdot), h(\cdot) \in \{-1, 1\}^n \rightarrow \mathbb{R}$, we define the *spectrum p-distance* between them as:

$$\mathbb{D}_p(g(\cdot), h(\cdot)) \triangleq \left(\sum_{S \subseteq [n]} |\hat{g}_S - \hat{h}_S|^p \right)^{1/p} \quad (10)$$

As there may have many candidates p for evaluating interpretation error and spectrum distance. In the following, we will investigate the most natural choice for p . As the Fourier expansion uniquely determined a Boolean function. We would like the distance between their expansion to have the same tendency as the interpretation error, thus the spectrum can encode enough information for reflecting the accuracy of interpretation. We shall first discuss the most “strict” case, i.e. the L_0 norm.

We shall introduce some notations for better understanding. Denote the support of an Boolean function f as $\text{supp}(f) \triangleq \{x \in \{-1, 1\}^n \mid f(x) \neq 0\}$. The support of Fourier coefficients (Fourier spectrum), is defined by $\text{supp}(\hat{f}) \triangleq \{S \subseteq [n] \mid \hat{f}(S) \neq 0\}$. The uncertainty principle for Boolean functions is stated as follows.

Proposition B.3 (Uncertainty Principle for Boolean functions (Gur & Tamuz, 2012; O’Donnell, 2014)). *For every nonzero function $f : \{-1, 1\}^n \rightarrow \mathbb{R}$,*

$$|\text{supp}(f)| \cdot |\text{supp}(\hat{f})| \geq 2^n.$$

Using the above Uncertainty Principle for Boolean functions, we can derive the following uncertainty principle for removal-based explanations:

Theorem 2. Assume $f, g \in \{-1, 1\}^n \rightarrow \mathbb{R}$ and $f \neq g$. When evaluated under L_0 norm, the interpretation error and spectrum distance have the following uncertainty principle:

$$\mathbb{I}_0(f, g) \mathbb{D}_0(f, g) \geq 1. \quad (11)$$

Proof. Taking μ as the uniform distribution, then $\mathbb{I}_0(f, g) = \frac{\sum_{x \in \{-1, 1\}^n} \mathbf{I}_{f(x) \neq g(x)}}{2^n} = \frac{|\text{supp}(f-g)|}{2^n}$. Note $\mathbb{D}_0(f, g) = \sum_{S \subseteq [n]} \mathbf{I}_{\hat{f}(S) \neq \hat{g}(S)} = |\text{supp}(\hat{f} - \hat{g})|$. The conclusion follows from Proposition B.3. \square

From the above derivation, we can see that L_0 norm is too strict for evaluating the differences between interpretations. Fortunately, the following proposition shows that if we can relax a bit, things may get much better.

Proposition B.4 (L_2 norm is natural). *When taking μ as uniform distribution. For $f, g \in \{-1, 1\}^n \rightarrow \mathbb{R}$, we have $\mathbb{I}_2(f, g) = \mathbb{D}_2(f, g)$.*

Proof. From the definition of $\mathbb{I}_2(f, g)$ and $\mathbb{D}_2(f, g)$. By Parseval’s identity, $\mathbb{I}_2^2(f, g) = 2^{-n} \sum_{x \in \{-1, 1\}^n} (f(x) - g(x))^2 = \sum_{S \subseteq [n]} (\hat{f}(S) - \hat{g}(S))^2 = \mathbb{D}_2^2(f, g)$. \square

C Harmonica Algorithm

To present the theoretical guarantees of the Harmonica algorithm, we introduce the following definition, which is slightly different from its original version in (Hazan et al., 2018).

Definition C.1 (Approximately sparse function). We say a function $f \in \{-1, 1\}^n \rightarrow \mathbb{R}$ is (ϵ, s, C) -bounded, if $\mathbb{E}[(f - \sum_{\chi_S \in C} \hat{f}(S) \chi_S)^2] \leq \epsilon$ and $\sum_S |\hat{f}(S)| \leq s$.

Here f is (ϵ, s, C) -bounded means it is almost readable and has bounded ℓ_1 norm. Our algorithm is slightly different from the original algorithm proposed by Hazan et al. (2018), but similar theoretical guarantees still hold, as stated below.

Theorem 3. Given $f \in \{-1, 1\}^n \rightarrow \mathbb{R}$ a $(\epsilon/4, s, C)$ -bounded function, Algorithm 1 finds a function g with interpretation error at most ϵ in time $O((T \log \frac{1}{\epsilon} + |C|/\epsilon) \cdot |C|)$ and sample complexity $T = \tilde{O}(s^2/\epsilon \cdot \log |C|)$.

Our proof is similar to the one in the original paper Hazan et al. (2018), with changes in the readable notion, which is now more flexible than being low order. First, recall the classical Chebyshev inequality.

Definition C.2 (Multidimensional Chebyshev inequality). Let X be an m dimensional random vector, with expected value $\mu = \mathbb{E}[X]$, and covariance matrix $V = \mathbb{E}[(X - \mu)(X - \mu)^T]$. If V is a positive definite matrix, for any real number $\delta > 0$:

$$\mathbb{P}\left(\sqrt{(X - \mu)^T V^{-1} (X - \mu)} > \delta\right) \leq \frac{m}{\delta^2}$$

Proof of Theorem 3. Let f be an $(\varepsilon/4, s, C)$ -bounded function written in the orthonormal basis as $\sum_S \hat{f}(S)\chi_S$. We can equivalently write f as $f = h + g$, where h is supported on C that only includes coefficients of magnitude at least $\varepsilon/4s$ and the constant term of the polynomial expansion of f .

Since $L_1(f) = \sum_S |\hat{f}_S| \leq s$, we know h is $4s^2/\varepsilon + 1$ sparse. The function g is thus the sum of the remaining $\hat{f}(S)\chi_S$ terms not included in h . Denote the set of bases that appear in C but not in g as R , so we know the coefficient of f on the bases in R is at most $\varepsilon/4s$.

Draw m (to be chosen later) random labeled examples $\{(z^1, y^1), \dots, (z^m, y^m)\}$ and enumerate all $N = |C|$ basis functions $\chi_S \in C$ as $\{\chi_1, \dots, \chi_N\}$. Form matrix A such that $A_{ij} = \chi_j(z^i)$ and consider the problem of recovering $4s^2/\varepsilon + 1$ sparse x given $Ax + e = y$ where x is the vector of coefficients of h , the i th entry of y equals y^i , and $e_i = g(z^i)$.

We will prove that with constant probability over the choice m random examples, $\|e\|_2 \leq \sqrt{\varepsilon m}$. Applying Theorem 5 in [Hazan et al. \(2018\)](#) by setting $\eta = \sqrt{\varepsilon}$ and observing that $\sigma_{4s^2/\varepsilon+1}(x)_1 = 0$ (see definition in the theorem), we will recover x' such that $\|x - x'\|_2^2 \leq c_2^2 \varepsilon$ for some constant c_2 . As such, for the function $\tilde{f} = \sum_{i=1}^N x'_i \chi_i$ we will have $\mathbb{E}[\|h - \tilde{f}\|^2] \leq c_2^2 \varepsilon$ by Parseval's identity.

Note, however, that we may rescale ε by constant factor $1/(2c_2^2)$ to obtain error $\varepsilon/2$ and only incur an additional constant (multiplicative) factor in the sample complexity bound. By the definition of g , we have

$$\|g\|^2 = \left(\sum_{S, \chi_S \notin C} \hat{f}(S)^2 + \sum_{S \in R} \hat{f}(S)^2 \right) \quad (12)$$

where each $\hat{f}(S)$ for $S \in R$ is of magnitude at most $\varepsilon/4s$. By Fact 4 in [\(Hazan et al., 2018\)](#) and Parseval's identity we have $\sum_R \hat{f}(R)^2 \leq \varepsilon/4$. Since f is $(\varepsilon/4, s, C)$ -concentrated we have $\sum_{S, \chi_S \notin C} \hat{f}(S)^2 \leq \varepsilon/4$. Thus, $\|g\|^2$ is at most $\varepsilon/2$. Therefore, by triangle inequality $\mathbb{E}[\|f - \tilde{f}\|^2] \leq \mathbb{E}[\|h - \tilde{f}\|^2] + \mathbb{E}[\|g\|^2] \leq \varepsilon$. It remains to bound $\|e\|_2$. Note that since the examples are chosen independently, the entries $e_i = g(z^i)$ are independent random variables. Since g is a linear combination of orthonormal monomials (not including the constant term), we have $\mathbb{E}_{z \sim D}[g(z)] = 0$. Here we can apply linearity of variance (the covariance of χ_i and χ_j is zero for all $i \neq j$) and calculate the variance

$$\text{Var}(g(z^i)) = \left(\sum_{S, \chi_S \notin C} \hat{f}(S)^2 + \sum_{S \in R} \hat{f}(S)^2 \right)$$

With the same calculation as Eqn. (12), we know $\text{Var}(g(z^i))$ is at most $\varepsilon/2$. Now consider the covariance matrix V of the vector e which equals $\mathbb{E}[ee^\top]$ (recall every entry of e has mean 0). Then V is a diagonal matrix (covariance between two independent samples is zero), and every diagonal entry is at most $\varepsilon/2$. Applying Theorem C.2 we have

$$\mathbb{P}\left(\|e\|_2 > \sqrt{\frac{\varepsilon}{2}}\delta\right) \leq \frac{m}{\delta^2}.$$

Setting $\delta = \sqrt{2m}$, we conclude that $\mathbb{P}(\|e\|_2 > \sqrt{\varepsilon m}) \leq \frac{1}{2}$. Hence with probability at least $1/2$, we have that $\|e\|_2 \leq \sqrt{\varepsilon m}$. From Theorem 5 in [\(Hazan et al., 2018\)](#), we may choose $m = \tilde{O}(s^2/\varepsilon \cdot \log n^d)$. This completes the proof. Note that the probability $1/2$ above can be boosted to any constant probability with a constant factor loss in sample complexity.

For the running time complexity, we refer to [\(Allen-Zhu & Yuan, 2016\)](#) for optimizing linear regression with ℓ_1 regularization. The running time is $O((T \log \frac{1}{\varepsilon} + L/\varepsilon) \cdot |C|)$, where L is the smoothness of each summand in the objective. Since each χ_S takes value in $\{-1, 1\}$, the smoothness is bounded by the number of entries in each summand, which is $|C|$. Therefore, the running time is bounded by $O((T \log \frac{1}{\varepsilon} + |C|/\varepsilon) \cdot |C|)$. \square

D Low-degree Algorithm

The low-degree algorithm is based on the concentration inequality, and it estimates the coefficient of each axis individually.

Algorithm 4 Low-degree

1. Given uniformly randomly sampled x_1, \dots, x_T , evaluate them on $f: \{f(x_1), \dots, f(x_T)\}$.
2. For any $\chi_S \in C$, let $\hat{g}_S = \frac{\sum_{i=1}^T f(x_i) \chi_S(x_i)}{T}$.
3. Output the polynomial $g(x) = \sum_{S, \chi_S \in C} \hat{g}_S \chi_S(x)$.

Theorem D.1 (Linial et al. (1993)). *Given any $\epsilon, \delta > 0$, assuming that function f is bounded by B , when $T \geq \frac{2B^2}{\epsilon^2} \log \frac{2|C|}{\delta}$, we have*

$$\Pr \left[\forall \chi_S \in C, \text{s.t.}, |\hat{g}_S - \hat{f}_S| \leq \epsilon \right] \geq 1 - \delta$$

Theorem D.1 was proved using the Hoeffding bound, and we included the proof here for completeness.

Proof. Since we are given T samples to estimate $\hat{f}(S)$ for every S , we can directly apply the Hoeffding bound (notice that the function is bounded by B):

$$\Pr \left(|\alpha_S - \hat{f}(S)| \geq \epsilon \right) \cdot |C| \leq 2 \exp \left(-\frac{2T\epsilon^2}{4B^2} \right) = 2 \exp \left(-\frac{T\epsilon^2}{2B^2} \right)$$

Notice that $T \geq \frac{2B^2}{\epsilon^2} \log \frac{2|C|}{\delta}$, we know the right hand size is bounded by $\frac{\delta}{|C|}$, so Theorem D.1 is proved. \square

Remarks. The theoretical guarantee of Harmonica assumes the target function f is approximately sparse in the Fourier space, which means most of the energy of the function (Fourier coefficients) is concentrated in the bases in C . This is not a strong assumption, because if f is not approximately sparse, it means f has energy in many different bases, or more specifically, the bases with higher orders. In other words, f has a large variance and is difficult to interpret. In this case, no existing algorithms will be able to give consistent and meaningful interpretations.

Likewise, although the Low-degree algorithm does not assume sparsity for f , it cannot learn all possible functions accurately as well. There are 2^n different bases, and if we want to learn the coefficients for all of them, the cumulative error for g is at the order of $\Omega(2^n \epsilon)$, which is exponentially large. This is not surprising due to the no free lunch theorem in the generalization theory, as we do not expect to be able to learn “any functions” without exponentially many samples.

E Discussion on the Existing Algorithms

In this section, we compare our approach with the existing techniques from the perspectives of interpretation error and truthfulness.

LIME (Ribeiro et al., 2016) Given an input x , Lime samples the neighborhood points based on a sampling distribution Π_x , and optimizes the following program:

$$\min_{g \in \mathcal{G}} L(f, g, \Pi_x) + \Omega(g)$$

where L is the loss function describing the distance between f and g on the sampled data points, \mathcal{G} is the set of readable functions (e.g. the set of linear functions), $\Omega(\cdot)$ is a function that characterizes the complexity of g . In other words, LIME tries to minimize the fitting error and simultaneously minimizes the complexity of g (which is usually the sparsity of the linear function). By minimizing L , LIME also works towards minimizing the interpretation error, but their approach is purely heuristic, without any theoretical guarantees. Although their readable function set can easily generalize to the set with higher order terms, the sampling distribution Π_x is not uniform, so it is difficult to incorporate the orthonormal basis into their framework. In other words, the model they compute is not truthful.

Attribution methods As we discussed in the introduction, attribution methods mainly focus on individual inputs, instead of the neighboring points. Therefore, it is difficult for the attribution methods to achieve low inconsistency, especially for first-order methods like SHAP (Lundberg & Lee, 2017) and IG (Sundararajan et al., 2017).

Consider SHAP (Lundberg & Lee, 2017) as a motivating example, illustrated in Fig. 3 for the task of sentiment analysis of movie reviews. In this example, the interpretations of two slightly different sentences are inconsistent. This inconsistency arises not only because the weights of each word differ significantly, but also because after removing the word “very” with a weight of 15.0%, the network’s output only drops by 6.6%. In other words, **the interpretation does not explain the network’s behavior even in a small neighborhood of the input.**

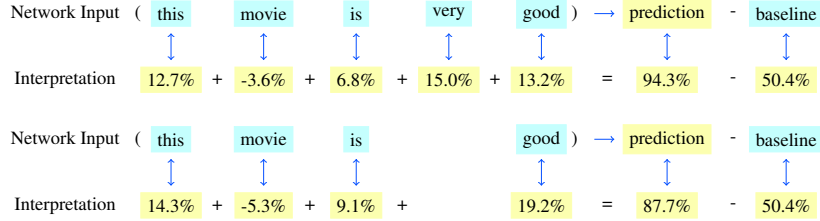


Figure 3: Interpretations generated by SHAP on a movie review.

For higher-order attribution methods, consistency can potentially be improved due to their enhanced representation power. The classical Shapley interaction index has the problem of not precisely fitting the underlying function, as observed by (Sundararajan et al., 2020), who proposed Shapley Taylor interaction index (Sundararajan et al., 2020) with better empirical performance. Shapley Taylor interaction index satisfies the generalized efficiency axiom, which says for all $f \in \{-1, 1\}^n \rightarrow \mathbb{R}$,

$$\sum_{S \subseteq [n], |S| \leq k} \mathcal{I}_S^k(f) = f([n]) - f(\emptyset)$$

We should remark that both the Shapley interaction index and Shapley Taylor interaction index were not originally designed for consistent interpretations, so they did not specify how to generalize the interpretation for the neighboring points. To this end, we make a global extension to the Shapley value based interpretation, that is, using Shapley interaction indices or Shapley Taylor interaction indices as the coefficients of corresponding terms of the polynomial surrogate function.

$$g(x_1, x_2, \dots, x_n) = f(\emptyset) + \sum_{x_i \in S, S \subseteq [n]} \mathcal{I}(f, S)$$

However, these higher-order Shapley value based methods all focus on the original Shapley value framework, so their interpretations are not truthful, i.e., not getting the exact coefficient of f even on the “simple bases”. Moreover, as we will show in our experiments, higher-order methods still incur high interpretation errors compared with our methods.

When applying Shapley value techniques for visual search, Hamilton et al. (2022) proposed an interesting and novel sampling + Lasso regression algorithm for efficiently computing higher order Shapley Taylor index in their experiments. However, their methods are based on a sampling probability distribution generated from permutation numbers, which is far from the uniform distribution. Additionally, their algorithm is based on the Shapley Taylor index, so their method is not truthful as well.

Emergence of self-explainability in foundation models In the groundbreaking work Sparks of AGI (Bubeck et al., 2023), the authors conducted comprehensive experiments on GPT-4’s self-explainability. Chain-of-thought (Wei et al., 2022) can be considered an interpretation provided by the model itself, although current LLMs are not always to be consistent or truthful. In the long run, however, this approach may represent the ultimate path to explainable AI. In the computer vision area, DINO (Caron et al., 2021; Oquab et al., 2023) emerges the ability of self-explanation provided by the attention map inside the model, which can be directly utilized as heatmap visualization or even applied to segmentation tasks.

Proposition E.1 (Omniscient LLM is the way). *An (infinitely) large (multi-modal) language model pre-trained using (infinitely) large corpus, with zero masking pre-training loss and generalization loss, which has been perfectly aligned to be truthful, is interpretable, efficient, and consistent.*

Proof. Self-explainability does not violate the Impossible Trinity since $f = g$, making it the only feasible approach to achieve interpretable, efficient, and consistent simultaneously.

Zero masking pre-training loss and generalization loss imply that the LLM has perfect knowledge of every problem.

Perfect alignment to be truthful ensures that its self-explanation is truthful, rendering it interpretable inherently (up to computable problems that can be represented by finite-length bits). \square

F Test with Low order Polynomial Functions

F.1 First order polynomial function

To investigate the performance of different interpretation methods, let us take a closer look at a 1st order polynomial function:

$$f_1(x_1, x_2, x_3) := \frac{1}{2}x_1 - \frac{1}{3}x_2 + \frac{1}{4}x_3$$

For this simple function, we can manually compute the outcome of each algorithm, as illustrated in Table 2. If the algorithm's output is correct, i.e., equal to the output of f_1 , we write a check mark. Otherwise, we write down the actual output of the given interpretation algorithm.

As we can see, all methods are consistent and efficient for all cases. In fact, all variants of Shapley indices degraded to 1st order Shapley values.

Algorithms	(-1, -1, -1)	(-1, -1, +1)	(-1, +1, -1)	(-1, +1, +1)	(+1, -1, -1)	(+1, -1, +1)	(+1, +1, -1)	(+1, +1, +1)
Ground Truth	-0.417	+0.083	-1.083	-0.583	+0.583	+1.083	-0.083	+0.417
LIME	✓	✓	✓	✓	✓	✓	✓	✓
SHAP	✓	✓	✓	✓	✓	✓	✓	✓
Shapley Interaction Index (1st order)	✓	✓	✓	✓	✓	✓	✓	✓
Shapley Taylor Index (1st order)	✓	✓	✓	✓	✓	✓	✓	✓
Faith-Shap (1st order)	✓	✓	✓	✓	✓	✓	✓	✓
Low-degree (1st order)	✓	✓	✓	✓	✓	✓	✓	✓
Harmonica (1st order)	✓	✓	✓	✓	✓	✓	✓	✓

Table 2: Interpretations by LIME, SHAP, Shapley Interaction Index, Shapley Taylor Index, Faith-Shap, Low-degree, and Harmonica on the 1st order polynomial function f_1 .

F.2 Second order polynomial function

In addition, let us take a closer look at a 2nd order polynomial function:

$$f_2(x_1, x_2, x_3) := \frac{1}{2}x_1 - \frac{1}{3}x_2 + \frac{1}{4}x_3 - \frac{1}{5}x_1x_2 + \frac{1}{6}x_1x_3 - \frac{1}{7}x_2x_3$$

For this simple function, we can manually compute the outcome of each algorithm, as illustrated in Table 3. If the algorithm's output is correct, i.e., equal to the output of f_2 , we write a check mark. Otherwise, we write down the actual output of the given interpretation algorithm.

As we can see, 2nd order interpretation algorithms, including Shapley Taylor index, Faithful Shapley, Low-degree, and Harmonica are consistent and efficient for all cases. Other methods can only fit a few inputs, the 2nd order Shapley interaction index misses all the cases because it is not efficient, and LIME misses all the cases because f_2 is not a linear function.

F.3 Third order polynomial function

Finally, we investigate the following 3rd order polynomial and present the result in Table 4.

$$f_3(x_1, x_2, x_3) := \frac{1}{2}x_1 - \frac{1}{3}x_2 + \frac{1}{4}x_3 - \frac{1}{5}x_1x_2 + \frac{1}{6}x_1x_3 - \frac{1}{7}x_2x_3 + \frac{1}{8}x_1x_2x_3$$

Algorithms	(-1, -1, -1)	(-1, -1, +1)	(-1, +1, -1)	(-1, +1, +1)	(+1, -1, -1)	(+1, -1, +1)	(+1, +1, -1)	(+1, +1, +1)
Ground Truth	-0.593	-0.140	-0.574	-0.693	+0.474	+1.593	-0.307	+0.240
LIME	-0.417	+0.083	-1.083	-0.583	+0.583	+1.083	-0.083	+0.417
SHAP	-0.240	+0.283	-1.250	-0.726	+0.726	+1.250	-0.283	
Shapley Interaction Index (2nd order)	-0.329	+0.171	-0.995	-0.781	+0.671	+1.505	-0.395	+0.152
Shapley Taylor Index (2nd order)	✓	✓	✓	✓	✓	✓	✓	✓
Faith-Shap (2nd order)	✓	✓	✓	✓	✓	✓	✓	✓
Low-degree (2nd order)	✓	✓	✓	✓	✓	✓	✓	✓
Harmonica (2nd order)	✓	✓	✓	✓	✓	✓	✓	✓

Table 3: Interpretations by LIME, SHAP, Shapley Interaction Index, Shapley Taylor Index, Faith-Shap, Low-degree, and Harmonica on the 2nd order polynomial function f_2 .

As we can see, Faith-Shap, Low-degree, and Harmonica are consistent and efficient for all cases. Other methods can only fit a few inputs, the 3rd order Shapley interaction index misses all the cases because it is not efficient, and LIME misses all the cases because f_3 is not a linear function.

Algorithms	(-1, -1, -1)	(-1, -1, +1)	(-1, +1, -1)	(-1, +1, +1)	(+1, -1, -1)	(+1, -1, +1)	(+1, +1, -1)	(+1, +1, +1)
Ground Truth	-0.718	-0.015	+0.449	-0.818	+0.599	+1.468	-0.432	+0.365
LIME	-0.417	+0.083	-1.083	-0.583	+0.583	+1.083	-0.083	+0.417
SHAP	-0.365	+0.242	-1.292	-0.685	+0.685	+1.292	-0.242	
Shapley Interaction Index (3rd order)	-0.485	+0.224	-0.943	-0.896	+0.724	+1.390	-0.510	+0.496
Shapley Taylor Index (3rd order)	✓	+0.194	-0.606	-0.970	+0.751	+1.625	-0.642	✓
Faith-Shap (3rd order)	✓	✓	✓	✓	✓	✓	✓	✓
Low-degree (3rd order)	✓	✓	✓	✓	✓	✓	✓	✓
Harmonica (3rd order)	✓	✓	✓	✓	✓	✓	✓	✓

Table 4: Interpretations by LIME, SHAP, Shapley Interaction Index, Shapley Taylor Index, Faith-Shap, Low-degree, and Harmonica on the 3rd order polynomial function f_3 .

G Experiment Settings

In this section, we will describe the detailed experimental settings. For the two language tasks, i.e., SST-2 and IMDb, we use the same CNN neural network. The model has a test accuracy of 85.6%. For the readability of results, we treat sentences as units instead of words – masking several words in a sentence may render the entire paragraph difficult to understand and even meaningless while masking a critical sentence has meaningful semantic effects. Therefore, the radius is defined as the maximum number of masked sentences for IMDb. The word embedding layer is pre-trained by GloVe (Pennington et al., 2014) and the maximum word number is set to 25,000. Besides the embedding layer, the network consists of several convolutional kernels with different kernel sizes (3, 4, and 5). After that, we use several fully connected layers, non-linear layers, and pooling layers to process the features. A Sigmoid function is attached to the tail of the network to ensure that the output can be seen as a probability distribution. Our networks are trained with an Adam (Kingma & Ba, 2015) optimizer with a learning rate of 0.01 for 5 epochs. For the vision task, we choose the official ResNet (He et al., 2016) architecture, which is available on PyTorch and we do not discuss the architecture details here.

Notice that our algorithm is a post-hoc model-agnostic interpretation algorithm, we only need to use the original neural network f to infer on given input as an oracle. This means that one can easily change the network architecture without any additional changes.

All the experiments are run on a server with 4 Nvidia 2080 Ti GPUs. More information about the runtime python environment and implementation details can be found in our code.

H Detailed Results on Interpretation Error

In this section, we provide interpretation error results under other norms (Fig. 4, 5, and 6) and the corresponding numerical results (Table 5, 6 and 7).

I Detailed Results on Harmonica-local

Fig. 7, 8 and 9 compares Harmonica-local and Harmonica algorithms on SST-2, IMDb and ImageNet, respectively. Here we set the radius of \mathcal{N}_x to be 4. The results reveal that Harmonica-local indeed performs better within the local region but fails to cover a far region.

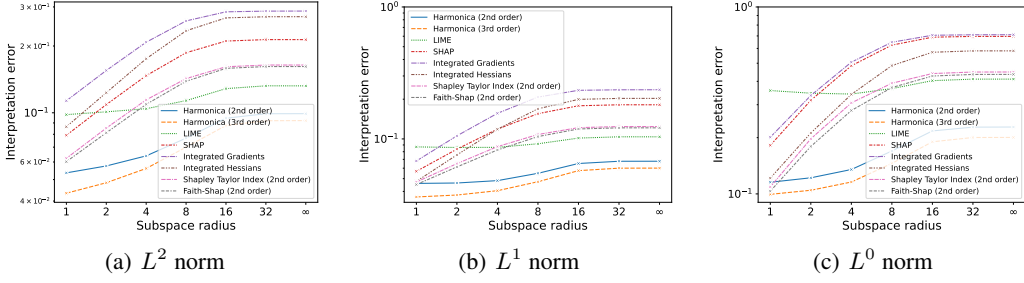


Figure 4: Visualization of interpretation error $\mathbb{I}_{p, \mathcal{N}_x}(f, g)$ evaluated on SST-2 dataset.

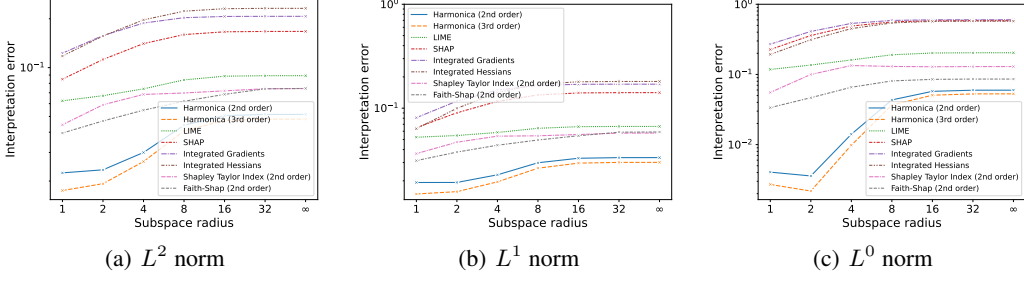


Figure 5: Visualization of interpretation error $\mathbb{I}_{p, \mathcal{N}_x}(f, g)$ evaluated on IMDb dataset.

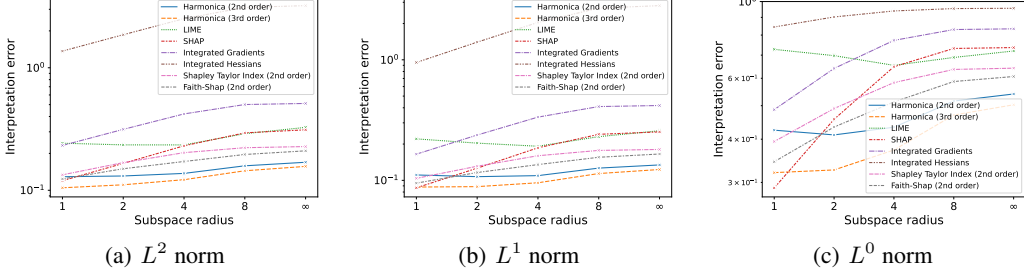


Figure 6: Visualization of interpretation error $\mathbb{I}_{p, \mathcal{N}_x}(f, g)$ evaluated on ImageNet dataset.

J Detailed Results on Truthful Gap

Estimating truthful gap For convenience, we define the set of bases C^d up to degree d as $C^d = \chi_S | S \subseteq [n], |S| \leq d$. We evaluate the truthful gap on the set of bases C^3 , C^2 , and C^1 . By definition in Eqn. (8), we have $\mathbb{T}_{V_C}(f, g) = \sum_{\chi_S \in C} \langle f - g, \chi_S \rangle^2 = \left(\mathbb{E}_{x \sim \{-1, 1\}^n} \left[(f(x) - g(x)) \sum_{\chi_S \in C} \chi_S(x) \right] \right)^2$.

Then we perform a sampling-based estimation of the truthful gap. Worth mentioning that since the size of set C^d satisfies $|C^d| = \sum_{i=0}^d \binom{n}{i}$ and the max number of words, sentences, or superpixels $n^* \leq 50$, $\sum_{\chi_S \in C} \chi_S(x)$, as the summation function of orthonormal basis, is easy to compute on every sample $x \in \{-1, 1\}^n$ (for n^* very large, we will perform another sampling step on this function).

Table 1 shows the C^3 truthful gap evaluated on different datasets. We can see that Harmonica outperforms all the other baseline algorithms. Due to space limitations, C^2 and C^1 results are provided in Appendix J.

radius	L^2 norm	L^1 norm	L^0 norm	radius	L^2 norm	L^1 norm	L^0 norm	radius	L^2 norm	L^1 norm	L^0 norm
1	0.0536	0.0460	0.1154	1	0.0434	0.0363	0.0995	1	0.0981	0.0870	0.3572
2	0.0576	0.0463	0.1219	2	0.0484	0.0376	0.1046	2	0.1010	0.0861	0.3458
4	0.0639	0.0483	0.1350	4	0.0561	0.0405	0.1157	4	0.1043	0.0863	0.3421
8	0.0768	0.0549	0.1696	8	0.0700	0.0474	0.1456	8	0.1135	0.0919	0.3659
16	0.0945	0.0651	0.2173	16	0.0876	0.0575	0.1900	16	0.1285	0.1015	0.4034
32	0.0990	0.0677	0.2275	32	0.0921	0.0600	0.2003	32	0.1323	0.1038	0.4111
∞	0.0991	0.0677	0.2279	∞	0.0922	0.0601	0.2005	∞	0.1322	0.1037	0.4112

Harmonica²
Harmonica³
LIME

radius	L^2 norm	L^1 norm	L^0 norm	radius	L^2 norm	L^1 norm	L^0 norm	radius	L^2 norm	L^1 norm	L^0 norm
1	0.0792	0.0568	0.1819	1	0.1133	0.0681	0.2010	1	0.0865	0.0477	0.1215
2	0.1089	0.0836	0.3167	2	0.1551	0.1055	0.3361	2	0.1232	0.0756	0.2118
4	0.1470	0.1186	0.4847	4	0.2081	0.1563	0.5066	4	0.1753	0.1183	0.3406
8	0.1865	0.1554	0.6252	8	0.2595	0.2075	0.6476	8	0.2343	0.1691	0.4859
16	0.2106	0.1783	0.6891	16	0.2852	0.2336	0.7058	16	0.2678	0.1994	0.5724
32	0.2137	0.1814	0.6958	32	0.2872	0.2357	0.7099	32	0.2709	0.2028	0.5823
∞	0.2137	0.1814	0.6961	∞	0.2874	0.2359	0.7105	∞	0.2711	0.2029	0.5823

SHAP
Integrated Gradients
Integrated Hessians

radius	L^2 norm	L^1 norm	L^0 norm	radius	L^2 norm	L^1 norm	L^0 norm	radius	L^2 norm	L^1 norm	L^0 norm
1	0.0623	0.0472	0.1090	1	0.0602	0.0451	0.1034	1	0.0865	0.0477	0.1215
2	0.0853	0.0649	0.1971	2	0.0813	0.0614	0.1795	2	0.1232	0.0756	0.2118
4	0.1144	0.0874	0.3069	4	0.1091	0.0824	0.2794	4	0.1753	0.1183	0.3406
8	0.1426	0.1081	0.3909	8	0.1387	0.1042	0.3707	8	0.2343	0.1691	0.4859
16	0.1612	0.1217	0.4404	16	0.1586	0.1190	0.4271	16	0.2678	0.1994	0.5724
32	0.1642	0.1241	0.4486	32	0.1616	0.1213	0.4356	32	0.2709	0.2028	0.5823
∞	0.1642	0.1240	0.4489	∞	0.1616	0.1213	0.4357	∞	0.2711	0.2029	0.5823

Shapley Taylor Index²
Faith-Shap²

Table 5: The interpretation error of Harmonica and other baseline algorithms evaluated on the SST-2 dataset for different neighborhoods with a radius ranging from 1 to ∞ under L^2 , L^1 and L^0 norms.

radius	L^2 norm	L^1 norm	L^0 norm	radius	L^2 norm	L^1 norm	L^0 norm	radius	L^2 norm	L^1 norm	L^0 norm
1	0.0225	0.0193	0.0041	1	0.0175	0.0149	0.0027	1	0.0624	0.0525	0.1175
2	0.0234	0.0193	0.0036	2	0.0193	0.0157	0.0022	2	0.0671	0.0546	0.1358
4	0.0300	0.0228	0.0141	4	0.0264	0.0195	0.0098	4	0.0740	0.0583	0.1606
8	0.0442	0.0298	0.0434	8	0.0407	0.0265	0.0367	8	0.084	0.0640	0.1903
16	0.0506	0.0330	0.0574	16	0.0472	0.0296	0.0506	16	0.0885	0.0664	0.2017
32	0.0515	0.0334	0.0596	32	0.0481	0.0301	0.0528	32	0.0892	0.0667	0.2033
∞	0.0515	0.0334	0.0597	∞	0.0481	0.0301	0.0529	∞	0.0892	0.0667	0.2033

Harmonica²
Harmonica³
LIME

radius	L^2 norm	L^1 norm	L^0 norm	radius	L^2 norm	L^1 norm	L^0 norm	radius	L^2 norm	L^1 norm	L^0 norm
1	0.0849	0.0650	0.2266	1	0.1228	0.0810	0.2702	1	0.1178	0.0635	0.1929
2	0.1123	0.0903	0.3589	2	0.1576	0.1169	0.4102	2	0.1567	0.0997	0.3125
4	0.1406	0.1162	0.4891	4	0.1882	0.1494	0.5333	4	0.1969	0.1415	0.4501
8	0.1598	0.1341	0.5610	8	0.2031	0.1657	0.5885	8	0.2227	0.1702	0.5423
16	0.1662	0.1402	0.5817	16	0.2067	0.1697	0.6004	16	0.2308	0.1795	0.5702
32	0.1671	0.1411	0.5842	32	0.2071	0.1702	0.6014	32	0.2319	0.1807	0.5739
∞	0.1671	0.1411	0.5843	∞	0.2071	0.1702	0.6015	∞	0.2319	0.1807	0.5738

SHAP
Integrated Gradients
Integrated Hessians

radius	L^2 norm	L^1 norm	L^0 norm	radius	L^2 norm	L^1 norm	L^0 norm
1	0.0444	0.0365	0.0554	1	0.0395	0.0313	0.0337
2	0.0590	0.0470	0.0999	2	0.0469	0.0378	0.0466
4	0.0684	0.0538	0.1339	4	0.0547	0.0440	0.0657
8	0.0698	0.0542	0.1300	8	0.0620	0.0494	0.0808
16	0.0719	0.0558	0.1287	16	0.0684	0.0543	0.0851
32	0.0741	0.0575	0.1294	32	0.0740	0.0588	0.0859
∞	0.0743	0.0577	0.1294	∞	0.0744	0.0590	0.0859

Shapley Taylor Index²
Faith-Shap²

Table 6: The interpretation error of Harmonica and other baseline algorithms evaluated on the IMDb dataset for different neighborhoods with a radius ranging from 1 to ∞ under L^2 , L^1 and L^0 norms.

Fig. 10 shows the truthful gap evaluated on SST-2 dataset. We can see that Harmonica achieves the best performance for C^2 and C^3 . For the simple linear case C^1 , Harmonica is almost as good as LIME.

radius	L^2 norm	L^1 norm	L^0 norm	radius	L^2 norm	L^1 norm	L^0 norm	radius	L^2 norm	L^1 norm	L^0 norm
1	0.1290	0.1108	0.4248	1	0.1048	0.0880	0.3202	1	0.2422	0.2208	0.7274
2	0.1308	0.1073	0.4116	2	0.1108	0.0887	0.3260	2	0.2347	0.2036	0.6976
4	0.1373	0.1094	0.4332	4	0.1220	0.0955	0.3723	4	0.2346	0.1918	0.6540
8	0.1584	0.1264	0.5156	8	0.1443	0.1139	0.4698	8	0.2897	0.2304	0.6893
∞	0.1693	0.1342	0.5405	∞	0.1566	0.1230	0.5030	∞	0.3261	0.2579	0.7196
Harmonica²				Harmonica³				LIME			
radius	L^2 norm	L^1 norm	L^0 norm	radius	L^2 norm	L^1 norm	L^0 norm	radius	L^2 norm	L^1 norm	L^0 norm
1	0.1197	0.0867	0.2892	1	0.2322	0.1650	0.4871	1	1.3681	0.9504	0.8443
2	0.1658	0.1261	0.4566	2	0.3141	0.2375	0.6406	2	1.8603	1.4006	0.9025
4	0.2306	0.1862	0.6483	4	0.4200	0.3346	0.7722	4	2.5168	2.0427	0.9394
8	0.2943	0.2409	0.7318	8	0.5010	0.4094	0.8300	8	3.1095	2.6844	0.9543
∞	0.3115	0.2523	0.7362	∞	0.5113	0.4177	0.8340	∞	3.2139	2.8140	0.9562
SHAP				Integrated Gradients				Integrated Hessians			
radius	L^2 norm	L^1 norm	L^0 norm	radius	L^2 norm	L^1 norm	L^0 norm	radius	L^2 norm	L^1 norm	L^0 norm
1	0.1337	0.1039	0.3939	1	0.1238	0.0948	0.3443	1	0.1238	0.0948	0.3443
2	0.1681	0.1309	0.4906	2	0.1499	0.1161	0.4338	2	0.1499	0.1161	0.4338
4	0.2028	0.1600	0.5830	4	0.1718	0.1351	0.5126	4	0.1718	0.1351	0.5126
8	0.2226	0.1771	0.6365	8	0.1960	0.1554	0.5872	8	0.1960	0.1554	0.5872
∞	0.2274	0.1804	0.6418	∞	0.2099	0.1654	0.6071	∞	0.2099	0.1654	0.6071
Shapley Taylor Index ²				Faith-Shap ²							

Table 7: The interpretation error of Harmonica and other baseline algorithms evaluated on the ImageNet dataset for different neighborhoods with a radius ranging from 1 to ∞ under L^2 , L^1 and L^0 norms.

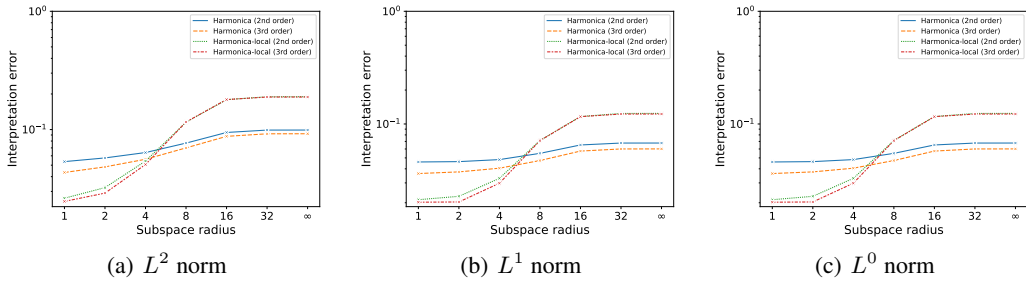


Figure 7: Visualization of interpretation error $I_{p, N_x}(f, g)$ evaluated on SST-2 dataset of algorithm Harmonica and Harmonica-local.

Fig. 11 shows the truthful gap evaluated on IMDb dataset under the same settings of SST-2 dataset. Fig. 12 shows the truthful gap evaluated on ImageNet dataset. We can see that Harmonica outperforms all the other baselines consistently.

K Detailed Results on Harmonica-anchor

K.1 Harmonica-anchor

Fig. 13, 14, and 15 show the interpretation error results evaluated on three datasets. All Harmonica-anchor algorithms further reduce the interpretation error compared to Harmonica. As we increase the number of anchors, the interpretation error slightly reduces, which is consistent with our intuition. Table 8, 9, and 10 show the numerical results.

K.2 Harmonica-anchor-constrained

Here we provide the interpretation error of Harmonica-anchor-constrained evaluated on SST-2 dataset in Fig. 16. As we increase the constraint coefficient λ_2 , the interpretation error increases, but still smaller than that of Harmonica.

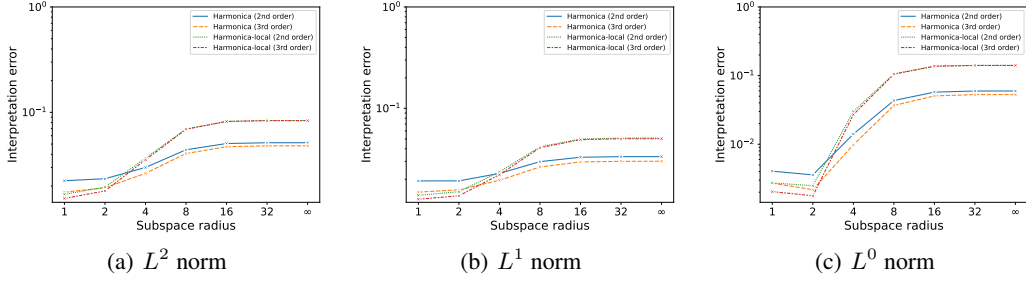


Figure 8: Visualization of interpretation error $\mathbb{I}_{p, N_x}(f, g)$ evaluated on IMDb dataset of algorithm Harmonica and Harmonica-local.

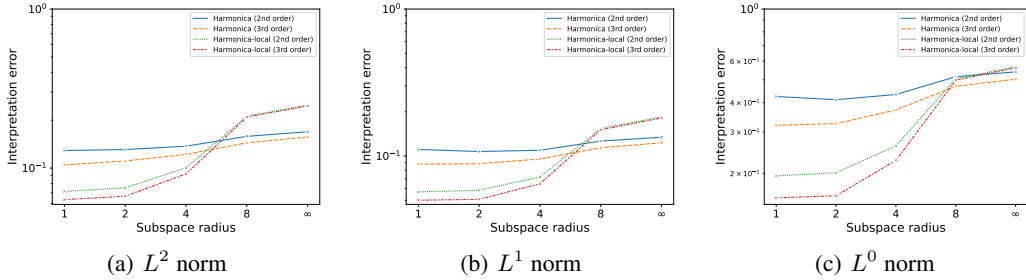


Figure 9: Visualization of interpretation error $\mathbb{I}_{p, N_x}(f, g)$ evaluated on ImageNet of algorithm Harmonica and Harmonica-local.

L Discussion on the Low-degree algorithm

From Theorem 3 and Theorem D.1, we know that the sample complexity of the Harmonica algorithm ($\tilde{O}(\frac{1}{\epsilon})$) is much more efficient than the Low-degree algorithm ($\tilde{O}(\frac{1}{\epsilon^2})$). Fig. 17 shows that when evaluating the interpretation error on SST-2 dataset, with the same sample size, the Harmonica algorithm outperforms the Low-degree algorithm by a large margin. We further increase the sample size for the Low-degree algorithm and see that its interpretation error gradually approaches that of Harmonica. However, even with 5x sample size, the Low-degree algorithm still gives a larger interpretation error compared with Harmonica. However, since exactly computing the Low-degree algorithm is extremely time-consuming, here we present the results using five times the sample size to show the calculation difficulty of the Low-degree algorithm.

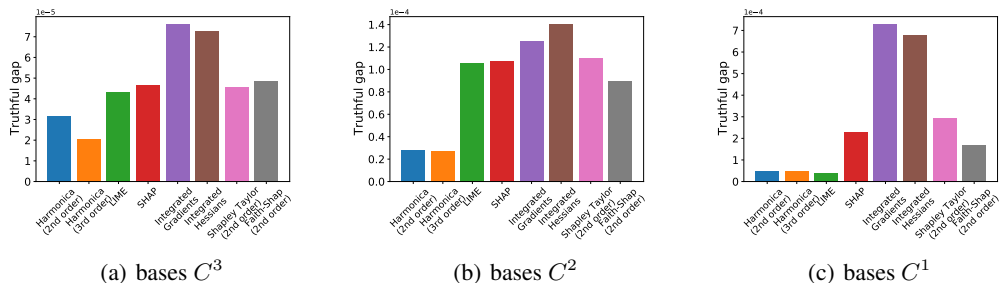


Figure 10: Visualization of truthful gap $\mathbb{T}_C(f, g)$ evaluated on SST-2 dataset.

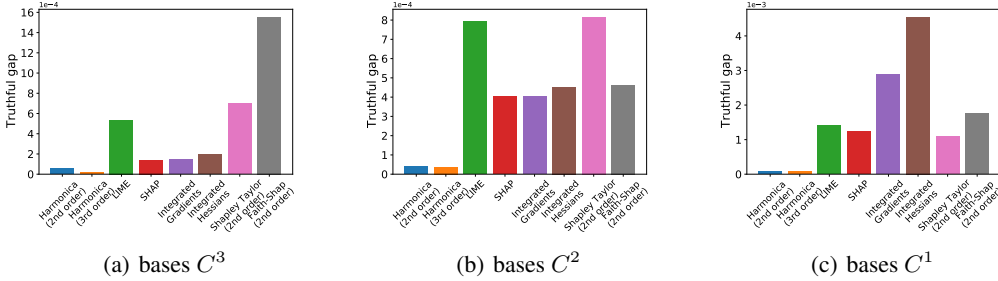


Figure 11: Visualization of truthful gap $\mathbb{T}_C(f, g)$ evaluated on IMDb dataset.

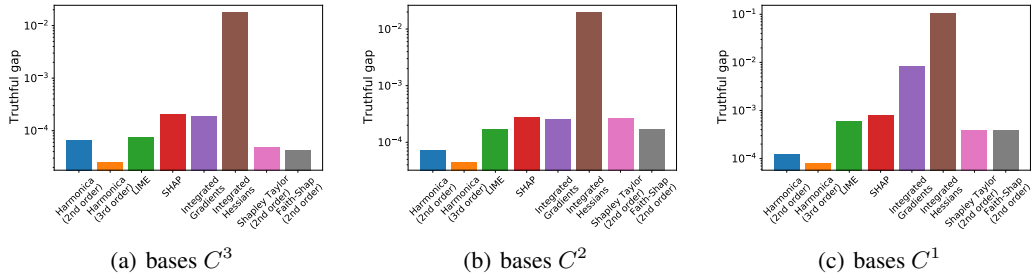


Figure 12: Visualization of truthful gap $\mathbb{T}_C(f, g)$ evaluated on ImageNet dataset.

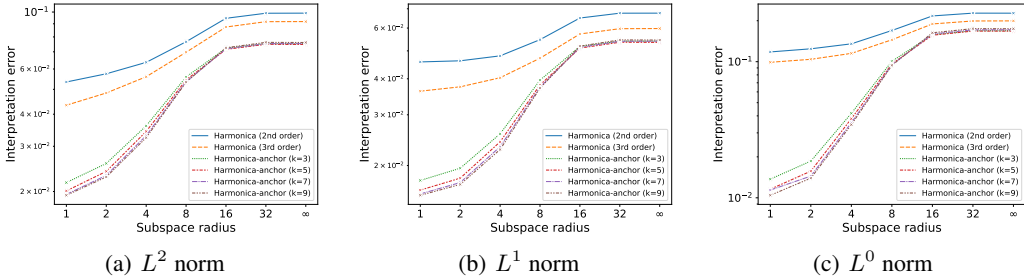


Figure 13: Visualization of interpretation error $\mathbb{I}_{p, N_x}(f, g)$ evaluated on SST-2 of Harmonica-anchor (2nd order) with different anchor number k .

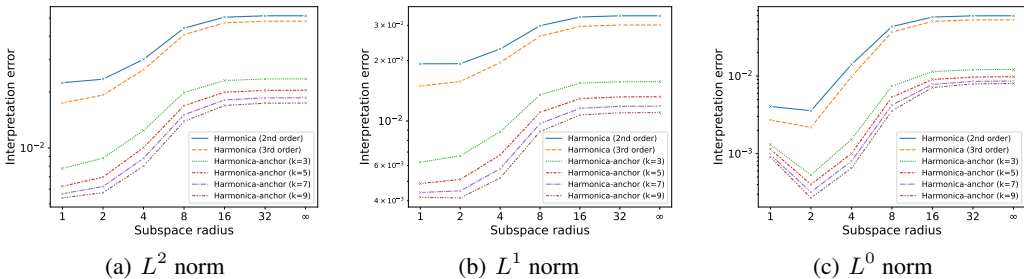


Figure 14: Visualization of interpretation error $\mathbb{I}_{p, N_x}(f, g)$ evaluated on IMDb of Harmonica-anchor (2nd order) with different anchor number k .

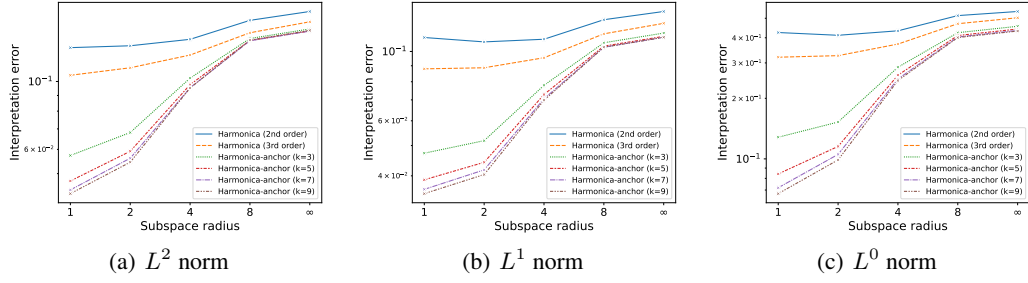


Figure 15: Visualization of interpretation error $\mathbb{I}_{p, \mathcal{N}_x}(f, g)$ evaluated on ImageNet of Harmonica-anchor (2nd order) with different anchor number k .

radius	L^2 norm	L^1 norm	L^0 norm
1	0.0217	0.0178	0.0137
2	0.0257	0.0196	0.0186
4	0.0360	0.0258	0.0417
8	0.0559	0.0396	0.1007
16	0.0723	0.0518	0.1579
32	0.0753	0.0541	0.1688
∞	0.0753	0.0541	0.1687

Harmonica-anchor ($k = 3$)

radius	L^2 norm	L^1 norm	L^0 norm
1	0.0201	0.0164	0.0116
2	0.0239	0.0181	0.0157
4	0.0343	0.0242	0.0381
8	0.0544	0.0381	0.0963
16	0.0715	0.0511	0.1565
32	0.0749	0.0536	0.1678
∞	0.0748	0.0535	0.1677

Harmonica-anchor ($k = 5$)

radius	L^2 norm	L^1 norm	L^0 norm
1	0.0195	0.0159	0.0114
2	0.0231	0.0175	0.0144
4	0.0330	0.0232	0.0356
8	0.0535	0.0374	0.0948
16	0.0719	0.0514	0.1598
32	0.0753	0.0540	0.1714
∞	0.0753	0.0540	0.1717

Harmonica-anchor ($k = 7$)

radius	L^2 norm	L^1 norm	L^0 norm
1	0.0193	0.0158	0.0104
2	0.0228	0.0172	0.0139
4	0.0324	0.0227	0.0345
8	0.0533	0.0371	0.0940
16	0.0726	0.0519	0.1631
32	0.0762	0.0546	0.1750
∞	0.0761	0.0545	0.1746

Harmonica-anchor ($k = 9$)

Table 8: The interpretation error of Harmonica-anchor algorithms evaluated on the SST-2 dataset for different k with a radius ranging from 1 to ∞ under L^2 , L^1 and L^0 norms.

radius	L^2 norm	L^1 norm	L^0 norm
1	0.0078	0.0062	0.0013
2	0.0088	0.0067	0.0005
4	0.0124	0.0088	0.0015
8	0.0199	0.0135	0.0074
16	0.0231	0.0154	0.0114
32	0.0235	0.0157	0.0121
∞	0.0236	0.0157	0.0121

Harmonica-anchor ($k = 3$)

radius	L^2 norm	L^1 norm	L^0 norm
1	0.0062	0.0049	0.0011
2	0.0070	0.0051	0.0004
4	0.0100	0.0068	0.0010
8	0.0169	0.0110	0.0053
16	0.0200	0.0129	0.0090
32	0.0204	0.0132	0.0097
∞	0.0204	0.0132	0.0098

Harmonica-anchor ($k = 5$)

radius	L^2 norm	L^1 norm	L^0 norm
1	0.0057	0.0044	0.0010
2	0.0062	0.0045	0.0003
4	0.0088	0.0058	0.0008
8	0.0151	0.0097	0.0042
16	0.0181	0.0116	0.0078
32	0.0186	0.0118	0.0085
∞	0.0186	0.0119	0.0086

Harmonica-anchor ($k = 7$)

radius	L^2 norm	L^1 norm	L^0 norm
1	0.0054	0.0042	0.0009
2	0.0057	0.0041	0.0003
4	0.0080	0.0052	0.0007
8	0.0139	0.0089	0.0036
16	0.0169	0.0107	0.0071
32	0.0174	0.0110	0.0079
∞	0.0174	0.0110	0.0080

Harmonica-anchor ($k = 9$)

Table 9: The interpretation error of Harmonica-anchor algorithms evaluated on the IMDb dataset for different k with a radius ranging from 1 to ∞ under L^2 , L^1 and L^0 norms.

radius	L^2 norm	L^1 norm	L^0 norm	radius	L^2 norm	L^1 norm	L^0 norm
1	0.0573	0.0473	0.1281	1	0.0473	0.0389	0.0842
2	0.0681	0.0518	0.1524	2	0.0592	0.0442	0.1153
4	0.1025	0.0779	0.2855	4	0.0976	0.0728	0.2608
8	0.1382	0.1066	0.4240	8	0.1361	0.1040	0.4104
∞	0.1485	0.1145	0.4562	∞	0.1462	0.1118	0.4422

Harmonica-anchor ($k = 3$) Harmonica-anchor ($k = 5$)

radius	L^2 norm	L^1 norm	L^0 norm	radius	L^2 norm	L^1 norm	L^0 norm
1	0.0442	0.0362	0.0719	1	0.0430	0.0351	0.0672
2	0.0561	0.0418	0.1053	2	0.0545	0.0404	0.0988
4	0.0954	0.0706	0.2496	4	0.0952	0.0698	0.2452
8	0.1358	0.1032	0.4036	8	0.1365	0.1032	0.4011
∞	0.1461	0.1110	0.4352	∞	0.1468	0.1110	0.4320

Harmonica-anchor ($k = 7$) Harmonica-anchor ($k = 9$)

Table 10: The interpretation error of Harmonica-anchor algorithms evaluated on the ImageNet dataset for different k with a radius ranging from 1 to ∞ under L^2 , L^1 and L^0 norms.

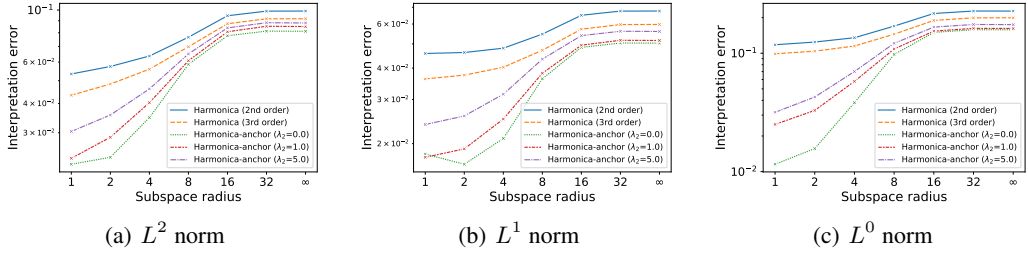


Figure 16: Visualization of interpretation error $\mathbb{I}_{p, N_x}(f, g)$ evaluated on SST-2 dataset of Harmonica-anchor-constrained (2nd order) with different coefficient λ_2 . Here all the Harmonica-anchor-constrained algorithms use $k = 5$.

radius	L^2 norm	L^1 norm	L^0 norm	radius	L^2 norm	L^1 norm	L^0 norm
1	0.0220	0.0182	0.0115	1	0.0234	0.0176	0.0250
2	0.0236	0.0166	0.0157	2	0.0287	0.0191	0.0329
4	0.0348	0.0210	0.0382	4	0.0403	0.0251	0.0579
8	0.0587	0.0363	0.0977	8	0.0608	0.0382	0.1086
16	0.0777	0.0484	0.1500	16	0.0808	0.0494	0.1538
32	0.0813	0.0504	0.1581	32	0.0853	0.0517	0.1623
∞	0.0812	0.0503	0.1579	∞	0.0851	0.0516	0.1620

Harmonica-anchor-constrained ($\lambda_2 = 0$)
Harmonica-anchor-constrained ($\lambda_2 = 1.0$)

radius	L^2 norm	L^1 norm	L^0 norm
1	0.0304	0.0238	0.0317
2	0.0357	0.0258	0.0427
4	0.0461	0.0315	0.0701
8	0.0650	0.0435	0.1214
16	0.0839	0.0539	0.1663
32	0.0883	0.0561	0.1750
∞	0.0881	0.0560	0.1745

Harmonica-anchor-constrained ($\lambda_2 = 5.0$)

Table 11: The interpretation error of Harmonica-anchor-constrained algorithms evaluated on the SST-2 dataset for different λ_2 with a radius ranging from 1 to ∞ under L^2 , L^1 and L^0 norms.

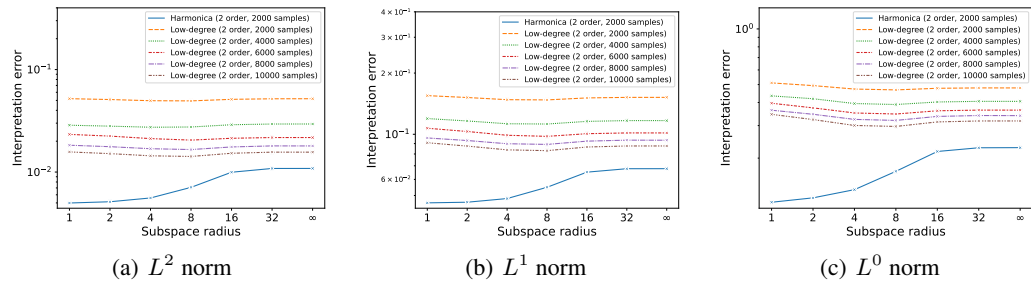


Figure 17: Visualization of interpretation error $\mathbb{I}_{p, N_x}(f, g)$ evaluated on SST-2 dataset, while Harmonica and Low-degree algorithms using different sample size varying from 2000 to 10000.